Cretaceous Episodic Extension in the South China Block, East Asia: Evidence From the Yuechengling Massif of Central South China

Yang Chu, Wei Lin, Michel Faure, Zhenhua Xue, Wenbin Ji, Zhentian Feng

HAL Id: insu-03595767
https://insu.hal.science/insu-03595767

Submitted on 3 Mar 2022

Tectonics

Cretaceous Episodic Extension in the South China Block, East Asia: Evidence From the Yuechengling Massif of Central South China

Yang Chu[1,2,3,4] [iD], Wei Lin[1,2] [iD], Michel Faure[5], Zhenhua Xue[6] [iD], Wenbin Ji[7], and Zhentian Feng[1,2]

[1]State Key Laboratory of Lithospheric Evolution, Institute of Geology and Geophysics, Chinese Academy of Sciences, Beijing, China, [2]College of Earth and Planetary Sciences, University of Chinese Academy of Sciences, Beijing, China, [3]Department of Earth Sciences, University of Durham, Durham, UK, [4]Innovation Academy of Sciences, Chinese Academy of Sciences, Beijing, China, [5]Institut des Sciences de la Terre d'Orléans, UMR 7327, Université d'Orléans, Orléans, France, [6]School of Earth Sciences, China University of Geosciences, Wuhan, China, [7]State Key Laboratory of Continental Dynamics, Department of Geology, Northwest University, Xi'an, China

Abstract In the Cretaceous, the subduction of the Izanagi/Paleo-Pacific plates beneath the South China Block (SCB) created a wide back-arc domain characterized by numerous extensional basins coeval with voluminous magmatism. The SCB witnessed the whole evolution by records of widespread extensional structures to accommodate the lithospheric stretching. In the interior of the SCB, the Yuechengling (YCL) Massif preserves a large, low-angle detachment fault, the Ziyuan Detachment (ZYD) at the western margin, and a high-angle ductile normal fault, the Tianhu Fault (THF), in the middle of the massif. Both faults display ductile shearing with top-to-the west kinematics but play different roles in two stages of extension. In the early stage at 140–120 Ma, the THF deformed the eastern YCL pluton at a temperature of ~350 °C, but the ZYD shows limited movement at this time. On the contrary, the later stage (100–85 Ma) is characterized by pervasive middle- to high-temperature deformation (~400–500 °C) and rapid exhumation along the ZYD, but the THF only underwent a near-surface brittle overprint. Across the SCB, the two-phase extension is widely recorded in other extensional structures and coincides with magmatic flare-ups at its eastern margin, suggesting episodic changes in the subduction dip. Combined with two compressional events that took place between the intervals of extension, the SCB experienced two cycles of compression-extension at 155–120 and 120–85 Ma. This periodicity is tentatively interpreted as a combined effect from the Izanagi/Paleo-Pacific subduction angle change and a thickening-foundering process in the arc region.

1. Introduction

Crustal extension is a common phenomenon in back-arc regions of subduction zones, such as the Aegean (Jolivet et al., 2013; Jolivet & Brun, 2010; Lister et al., 1984; Ring et al., 2010) and western North America (Davis & Coney, 1979; Davis & Lister, 1988; Sonder & Jones, 1999; Wernicke, 1981). Within extensional tectonics, normal faults play an important role to accommodate the stretching of continental crust by exhuming middle-lower crustal units. First described in the Basin and Range province, metamorphic core complexes (MCCs) are now considered as best indicators of highly extended continental crust and are characterized by low-angle normal faults that juxtapose sedimentary rocks of the hanging wall and highly strained, metamorphic rocks of the footwall (Crittenden et al., 1980; Davis & Coney, 1979; Lister & Davis, 1989; Wernicke, 1981). These low-angle normal faults, or detachments, commonly evolve from gently dipping, ductile extensional shear zones in the lower/middle crust and transform into discrete brittle faults at surface. Detachment and its supradetachment basin have been widely used to identify extensional structures, and further studies on structural evolution and geochronology can constrain the timing and amount of crustal stretching (Augier et al., 2015; Jolivet et al., 2013; Lin et al., 2008; Lin et al., 2013; Lin et al., 2013).

A major portion of East China has experienced large-scale extension within back-arc regions of the Late Mesozoic Paleo-Pacific subduction system. This may also lead to the spectacular destruction of the North China Block (NCB) that removed a large amount of lithospheric mantle since the Mesozoic (Chen et al., 2009; Lin & Wang, 2006; Wu et al., 2019; Zhu et al., 2011). The South China Block (SCB), which was amalgamated with the NCB by the Qinling-Dabie orogeny, displays a similar extensional scenario (Ji, Lin, Faure, Shi, et al., 2017; Li et al., 2014). The Paleo-Pacific oceanic plate subducted westward beneath the SCB, where

voluminous plutonic and volcanic rocks were widespread in the central and eastern regions from 160 to 90 Ma (Li & Li, 2007; Zhou et al., 2006). Despite intermittent short-lived compression, extensional structures dominated the tectonic framework of the Late Mesozoic SCB, including (half-) graben basins and brittle normal faults or detachments (Li et al., 2014; Shu et al., 2009). Recent studies have reported several detachments within MCCs or extensional domes in this region, and those detailed work on field mapping, structural analysis, and geochronological/thermochronological dating constrain the deformation pattern and episodes of activities of those detachments (Ji et al., 2018; Li et al., 2013; Wei et al., 2016; Zhu, Xie, et al., 2010).

To better recover the general history of extension in the SCB, the knowledge of timing, kinematics, exhumation amount and rate, and spatial variation is critical. However, compared with the well-constrained tectonic evolution of the MCCs in the NCB (Lin et al., 2008; Lin, Faure, et al., 2013; Liu et al., 2005; Wang et al., 2011; Zhu et al., 2015), not only variable kinematics has been demonstrated in different MCCs/domes of the SCB (e.g., Faure et al., 1996; Lin et al., 2000; Zhu, Xie, et al., 2010; Li et al., 2014; Wei et al., 2016; Ji, Faure, et al., 2018), but the temporal-spatial distribution of extensional structures also provides a more complex story that contains episodic deformation with ill-defined boundaries of this extensional province (Ji et al., 2014; Figure 1). Notwithstanding the complication of the Late Mesozoic tectonics in the SCB, more pieces of evidence are accumulated with the timing, amount, and geodynamic setting of extension than were known before. In the central SCB, the Yuechengling Massif develops a large-scale low angle detachment and a hanging wall Cretaceous basin. As the westernmost extensional structure, it occupies a significant position to help us delineate the boundary of the extensional province, and its deformation history also provides important clues to reconstruct the precise temporal sequence of extension. This paper presents a multidisciplinary study of this detachment and adjacent regions to complete the regional deformation scheme and shed light on the tectonic evolution of the Cretaceous back-arc extension in the SCB.

2. Geological Setting

The SCB is a composite landmass that includes different tectonostratigraphic units with distinct rock formations and tectonic histories. As the remnant of the Neoproterozoic subduction and collision, the Jiangshan-Shaoxing Fault zone (JSF in Figure 1) and ophiolitic rocks witness the amalgamation between two Precambrian blocks (Charvet et al., 1994; Shu & Charvet, 1996; Wang et al., 2013), the Yangtze Block to the west and the Cathaysia Block to the east (Figure 1). This event has been mostly concealed by Paleozoic and Mesozoic sedimentary rocks, or erased by later tectonic reworking. After the Neoproterozoic collisional orogeny, two Phanerozoic intracontinental orogenic events (Early Paleozoic and Triassic) involved different parts of the SCB, leading to a distinct tectonic segmentation (Chu & Lin, 2014; Faure et al., 2009).

The eastern part of the SCB experienced intense Early Paleozoic deformation-metamorphism-magmatism, which not only reworked most of the Neoproterozoic structures but obliterated Neoproterozoic petrological records by amphibolite-facies or granulite-facies metamorphism, migmatization, and widespread intrusions (Charvet et al., 2010; Chu & Lin, 2014; Faure et al., 2009; Li et al., 2010; Li et al., 2016). In the absence of a magmatic arc, subduction complex, and ophiolites, this orogeny is interpreted as an intracontinental event that may have initiated as early as ~465 Ma (Charvet et al., 2010; Chu & Lin, 2014). The synmetamorphic ductile deformation yields U-Pb ages at 460–440 Ma indicative of the culmination of the compression (Charvet et al., 2010; Li et al., 2010 ; Wang et al., 2012). Synorogenic and postorogenic granitoids widely spread in the whole orogen from 460 to 420 Ma, but the demise of the orogen is recorded by ^{40}Ar-^{39}Ar cooling ages at 390–380 Ma (Chu & Lin, 2014; Faure et al., 2009). The Triassic deformation is poorly developed, but we can still find some clues of deformation in Late Paleozoic to Middle Triassic rocks unconformably overlain by Late Triassic terrigenous deposits (Li et al., 2010; Wang et al., 2012). In contrast to the limited effect of the Early Mesozoic compression, the Late Mesozoic arc-related magmatism controlled by the Paleo-Pacific subduction is dominant in the coastal region of the SCB. Volcanic and plutonic rocks overlie on or intrude into pre-Jurassic rocks of this region (Li, 2000; Li et al., 2014; Zhou & Li, 2000).

The western part of the SCB shows a different tectonic scenario. Together with the Sichuan Basin that represents the core of this Precambrian continental fragment, the entire block received a continuous Paleozoic-Early Mesozoic deposition with over 10 km thick of sandstone, siltstone, mudstone, and limestone (BGMRJX, 1984; BGMRGX, 1985; BGMRHN, 1988). Except the Late Silurian to Early Devonian
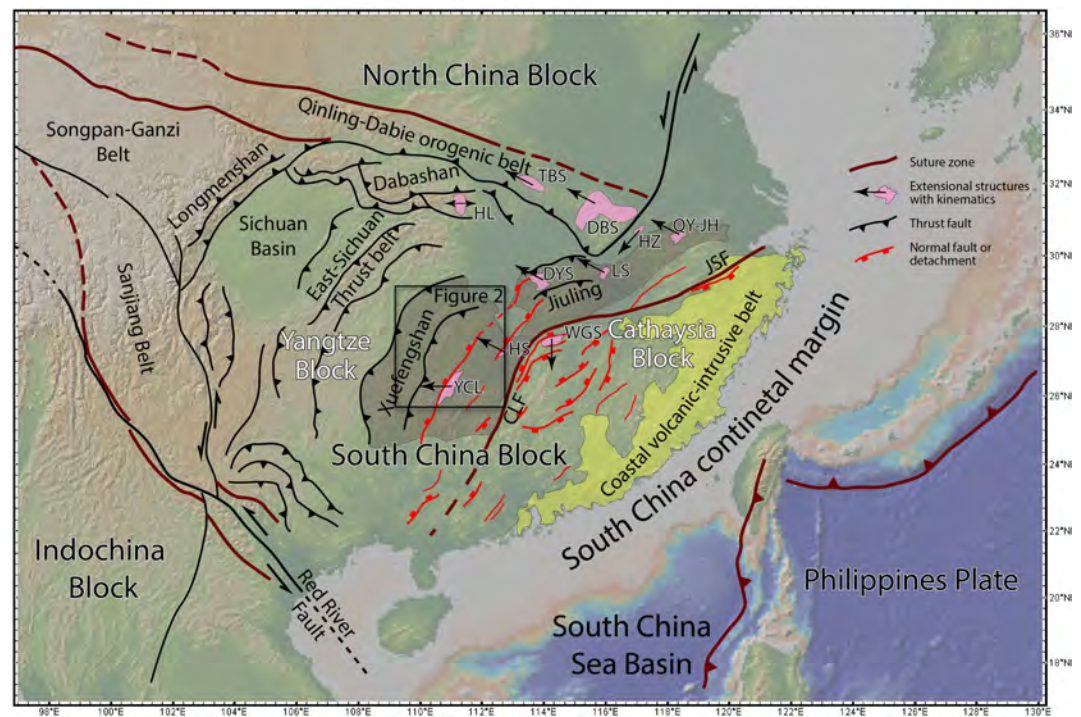
Figure 1. Tectonic map of the South China Block and adjacent regions. Mesozoic structures including fold-thrust belts and extensional domes/metamorphic core complexes are highlighted on this map. The base map made with GeoMapApp (http://www.geomapapp.org). JSF: Jiangshan-Shaoxing Fault. CLF: Chenzhou-Linwu Fault. Extensional domes/metamorphic core complexes: DBS: Dabieshan. DYS: Dayunshan. HL: Huangling. HS: Hengshan. HZ: Hongzhen. LS: Lushan. TBS: Tongbaishan. QY-JH: Qingyang and Jiuhua. WGS: Wugongshan. YCL: Yuechengling.

unconformity or disconformity in the eastern part of the Yangtze Block, most of the area escaped the Early Paleozoic high-temperature metamorphism and ductile shearing, but folded strata are common because of the foreland thrust belt of the intracontinental Wuyi-Yunkai orogeny, that centers on the eastern SCB (Chu & Lin, 2014; Li et al., 2010).

Mesozoic compressional events play a significant role in shaping the architecture of the Yangtze Block. The Early Mesozoic (Middle to Late Triassic) compression created the NE-SW to E-W trending intracontinental Xuefengshan Belt to the northwest of the Chenzhou-Linwu Fault and Jiangshan-Shaoxing Fault (Figure 1; Chu, Faure, Lin, & Wang, 2012; Chu, Faure, Lin, Wang, & Ji, 2012; Chu & Lin, 2018; Faure et al., 2016), but the west tectonic front is ambiguous, because this belt is partly modified by a second compressional phase during the Jurassic-Early Cretaceous (Yan et al., 2003, 2009). Multistage tectonics that includes Early Mesozoic and Late Mesozoic events also resulted in episodic contraction and exhumation of the circum-Sichuan Basin belts (Yan et al., 2011; Dong et al., 2013; Tian et al., 2016; Xue et al., 2017).

The two parts of the SCB display contrasting tectonostratigraphy, but, as a matter of fact, they share similar tectonic histories with variable deformation intensity. Since the Late Mesozoic, the Paleo-Pacific subduction at the eastern continental margin of the SCB started to influence the surface stress field in a wide region from the coastal regions to the Xuefengshan Belt at the center. Then arc-related magmatism and regional extension became the major characteristics in response to the interaction between the two plates (Zhou et al., 2006; Zhou & Li, 2000). The first magmatic flare-up initiated at ~160 Ma and invoked gigantic granitic intrusions in the eastern SCB (Li et al., 2014). Two Cretaceous magmatic pulses occurred with widespread volcanism and mineralization. Contemporaneous with the Cretaceous magmatism, detachments or high-angle normal faults controlled most extensional basins in which continental red beds were deposited (Shu et al., 2009). Some pretectonic and syntectonic granitic plutons were also deformed under subsolidus conditions by these detachments (Ji, Faure, et al., 2018; Wei et al., 2014), but most of the structures can be classified as extensional domes/MCCs (Figure 1), including Hengshan (Li et al., 2013; Wei et al., 2016), Lushan (Lin et al., 2000; Zhu, Xie, et al., 2010), Hongzhen (Zhu, Yang, & Wang, 2010), Wugongshan (Faure et al., 1996), and Yuechengling,

which were subjected into pervasive ductile deformation. However, two kinematics include NE-SW and NW-SE stretching characterize those extensional structures (Ji, Faure, et al., 2018; Li et al., 2013; Zhu, Xie, et al., 2010), indicating a heterogeneous pattern that accommodates the large-scale crustal extension.

3. Tectonic Units of the Yuechengling Massif and Preextension Deformation

The Yuechengling Massif mainly consists of the Early Paleozoic Miaoershan and Yuechengling plutons, metamorphosed Neoproterozoic rocks, and Paleozoic-Mesozoic sedimentary rocks (Figures 2 and 3). The two plutons are almost equally sized and intruded into pre-Devonian metasedimentary rocks. The Miaoershan pluton is a coarse-grained biotite granite with localized ductile deformation along its western margin; the Yuechengling pluton, which has similar mineral composition, is intensively deformed and sheared. Radiometric ages show that the Miaoershan and Yuechengling plutons crystallized at 412 ± 4 and 424 ± 3 Ma, respectively (Chu, Lin et al., 2012).

The Ziyuan Detachment (ZYD) separates the western hanging wall from the eastern footwall that yield distinct deformation features (Figure 3a). The hanging wall includes from top to bottom: the Cretaceous Xining Basin, Paleozoic to Early Mesozoic strata, Early Paleozoic Miaoershan pluton, and metamorphosed Neoproterozoic sandstone/mudstone. These greenschist-amphibolite facies metamorphic rocks form the ductile decollement zone developed during the Triassic intracontinental Xuefengshan orogeny (Chu, Faure, Lin, Wang, & Ji, 2012). During the Cretaceous activity of the ZYD, the hanging wall only recorded brittle deformation by faults and joints.

The footwall consists of the deformed Yuechengling pluton and Paleozoic and Mesozoic limestone sandstone (Figure 3a). Compared with the hanging wall, the ductile deformation in the footwall is localized immediately below the ZYD, suggesting a direct link to the Cretaceous extension. Eastward from the detachment, the structures related to the Triassic intracontinental orogeny can be traced because of the weak overprint by the extensional tectonics (Chu, Faure, Lin, & Wang, 2012). In the following, we shall focus on the structural analysis of the deformation linked to the Cretaceous extensional event.

4. Structural Analysis

4.1. The Ziyuan Detachment

Extending NE-SW, the Ziyuan Detachment represents the largest tectonic discontinuity in this region (Figure 3a), juxtaposing ductilely deformed and metamorphosed middle crustal rocks of the footwall with unmetamorphosed upper crustal rocks of the hanging wall. The activity of the detachment resulted in tens to hundreds of meters-thick fault zone, containing from west to east a combination of faulted rocks that are fault breccia, silicified cataclasite, mylonitic granite, and sheared granite (inset in Figure 4). The structure of the deformed granite will be presented in the following section; only the rocks involved in the detachment are analyzed here.

The uppermost part of the detachment consists of fault-related breccia. Along the entire detachment, tectonic breccia develops continuously at the base of the Cretaceous Xinning Basin or Paleozoic rock formations. The thickness of the brecciated zone varies from 1 m to tens of meters throughout the length of the detachment. Depending on the different rock types, from Cretaceous red sandstone and conglomerate to Paleozoic limestone, the breccia shows distinct appearances. To the east of the Xinning Basin, the lower sedimentary formation contains conglomerate with rock fragments enclosed in pelitic matrix at the base of the extensional basin. This conglomerate was then involved into intense brittle deformation with fractures (Figure 5a). As the detachment activity continued, rock fragments were further crushed into small pieces and formed a gouge zone above which a new brecciated zone was produced. In places where the hanging wall consists of limestone, fluids that migrated along the main fault zone were injected into rock fissures and provoked rock fragmentation and fault brecciation (Figure 5b). The density of the fractures or veins increases toward the detachment, and multiple stages of injection of calcite or quartz fluid can be observed due to the repeated fault motion.

Beneath the breccia, near the main detachment plane, intensive fluid infiltration formed silicified cataclasite (Figures 5c and 5d). The thickness of this cataclasite ranges from 1 to 6 m, but along-strike variation in fluid supply and fault activity led to discontinuous occurrences of the silicified cataclasite. On top of the granite,
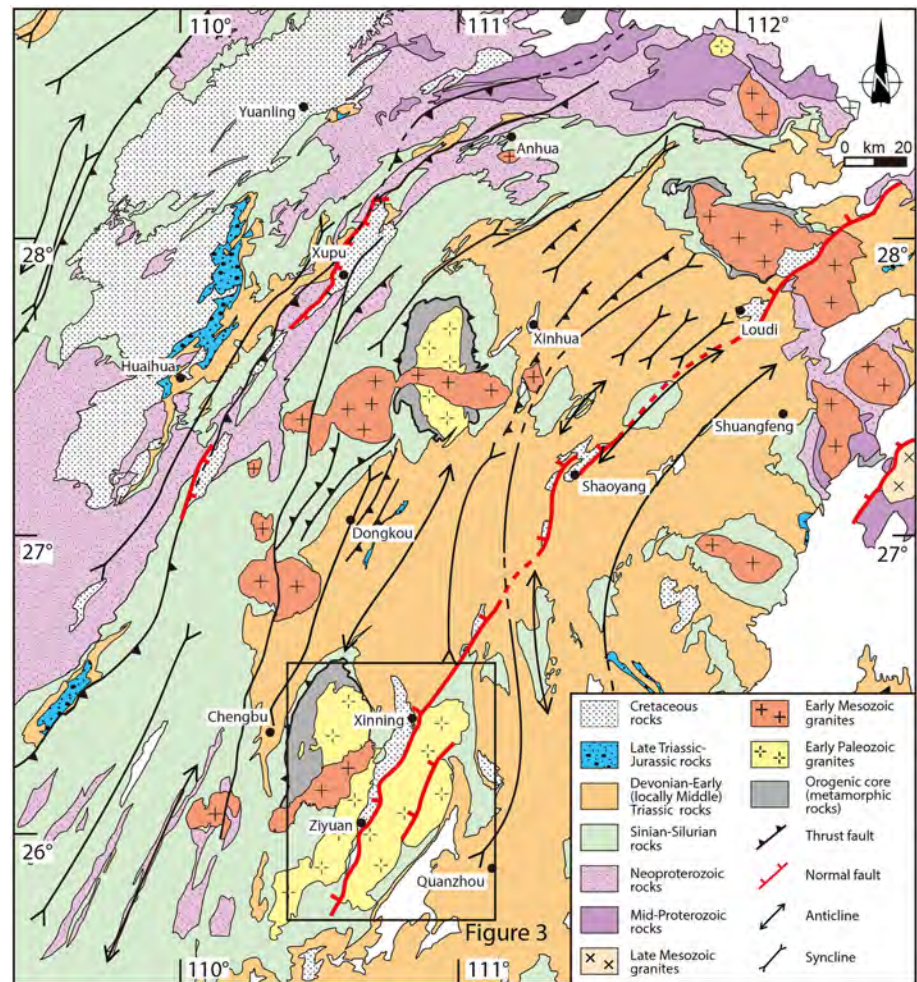
Figure 2. Structural map of the Xuefengshan Belt modified after Chu, Faure, Lin, and Wang (2012). Important normal faults/detachments are highlighted. The box shows the location of the Yuechengling Massif presented in Figure 3.

cataclasite exposures display a light green color, highly fractured appearance, and early foliation or other planar structures has been totally distorted by protracted brittle faulting along the detachment (Figure 5c). Shear bands spaced in 10–30 cm gently dip to the west and cut the cataclasite, in agreement with the overall kinematics of the detachment. Silicified cataclasite consists of 90% of quartz grains and minor dark minerals, which completely replaced the original mineralogy by fluid-rock interaction (Figure 5d). At the microscopic scale, the highest strain was localized in 0.5- to 1-mm-wide cataclastic zones in which quartz grains were crushed to less than 10 μm (Figure 5e). These small-scale shear zones developed in the cataclasite document heterogeneity of accumulated strain (Figure 5f). Coarse quartz grains sometimes are ductilely deformed with undulatory extinction in the core and initial bulging at grain boundaries, respectively, suggesting low-temperature deformation in a brittle-ductile transition zone (Figure 5f).

Along the boundary between the YCL pluton and the Cretaceous Xinning Basin, the detachment plane can be well traced with smooth surfaces and conspicuous slickenlines (Figure 5g). This contact is preserved with a silicate-rich layer coating the surface, which results from fluid penetration along the fault plane. This process facilitates the persistent fault activity and in turn gives rise to more infiltration of fluid from the deeper parts. The detachment plane dips to the west at angles between 20° and 40°. Some surfaces carry decimetric-scale corrugation parallel to the motion of the fault. On the detachment plane, slickenlines made of quartz fibers and rods of quartz aggregates show a consistent top-to-the west sense of slip (Figure 5g). When approaching the subsurface, the detachment itself and its adjacent rocks, including cataclastic granites and breccia, are cut by secondary normal faults with medium to high angle dipping to the west, and similar kinematics is indicated by dip-slip striations and steps (Figure 5h).
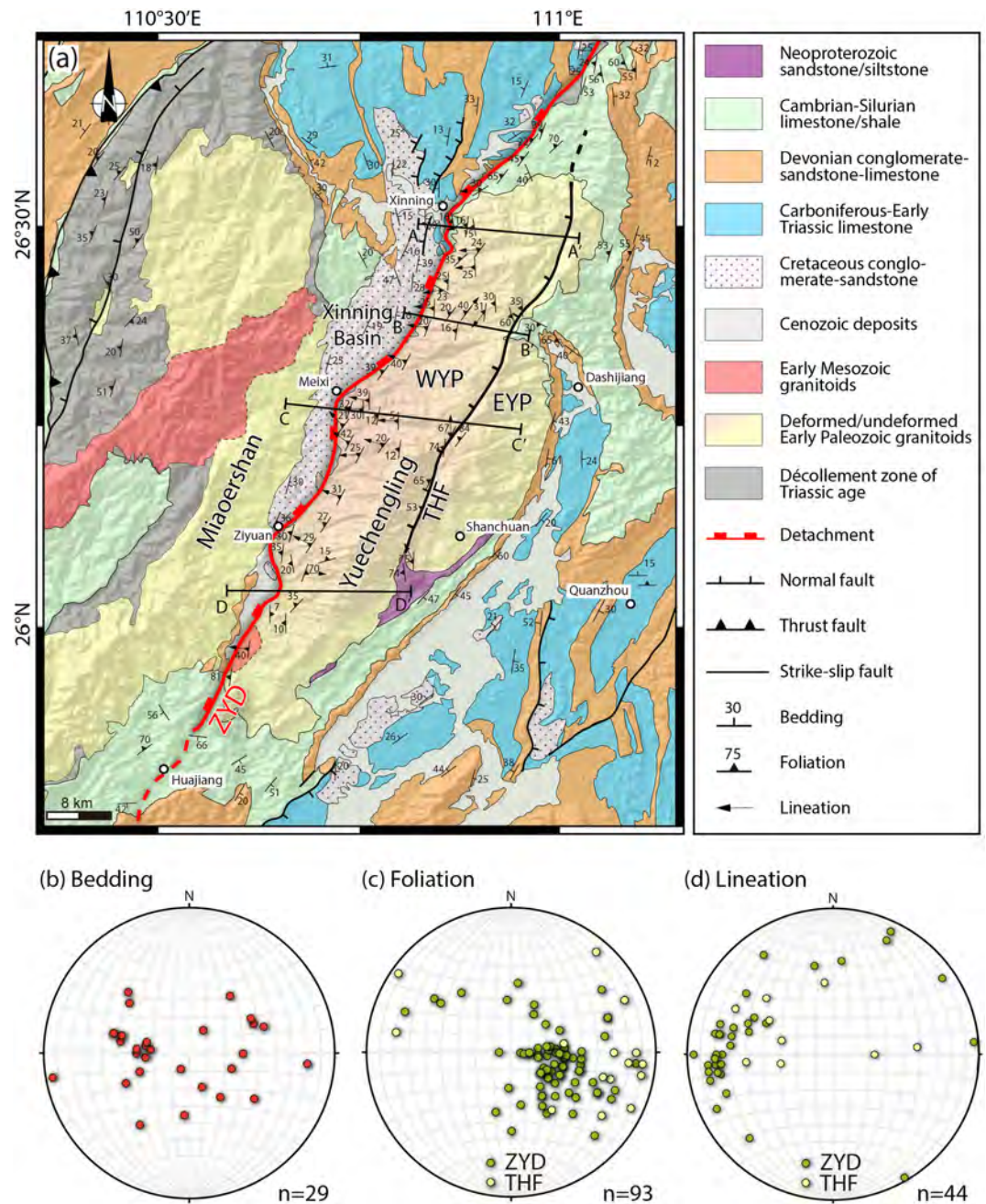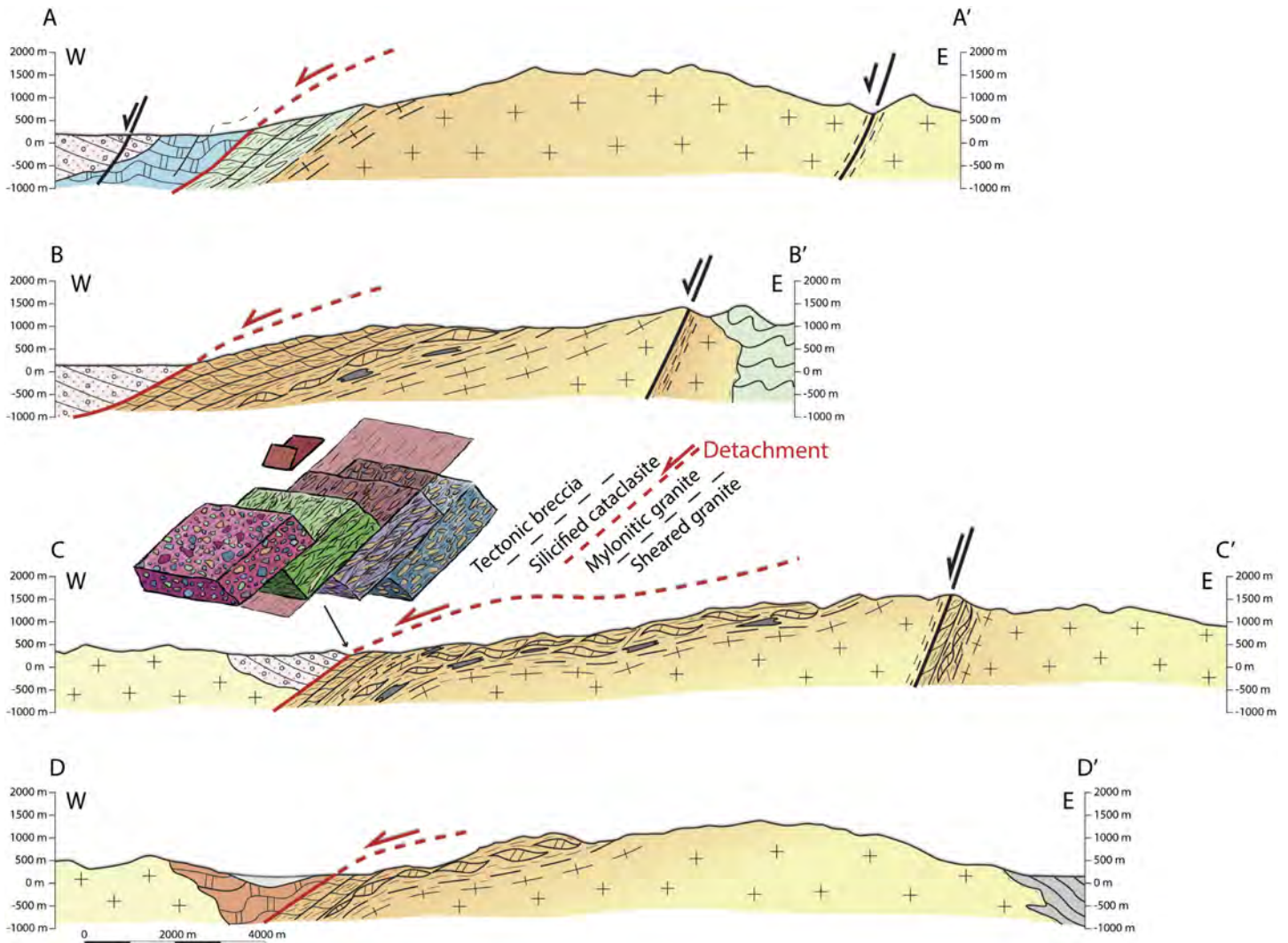
Figure 3. (a) Geological map of the Yuechengling Massif and its adjacent regions. Lithological outlines are based on our field observations and existing maps (BGMRHN, 1988; Chu, Faure, Lin, & Wang, 2012; Chu, Faure, Lin, Wang, & Ji, 2012). Structural foliation and lineation based on our fieldwork show the general architecture of the Yuechengling Massif with north striking foliation and E-W trending lineation. EYP: Eastern Yuechengling pluton. WYP: Western Yuechengling pluton. ZYD: Ziyuan Detachment. THF: Tianhu Fault. (b–d) Stereographic plots of structural elements from the Yuechengling Massif in Schmidt's lower hemisphere equal-area projection. ZYD: Ziyuan Detachment. THF: Tianhu Fault. (b) Poles to bedding of undeformed/weakly deformed rocks. (c) Poles to foliation. (d) Lineation.

4.2. Footwall of the Ziyuan Detachment

4.2.1. Deformation in the Western Yuechengling Pluton

The YCL pluton, as the major portion of the footwall, shows an obvious strain gradient decreasing from west to east. The ductile shear zone is separated from the isotropic granite by a high-angle normal fault, the THF, in the middle the granite, which allows us to subdivide the pluton into two parts, the Eastern

AGU
100
ADVANCING EARTH
AND SPACE SCIENCE

Tectonics

10.1029/2019TC005516

Figure 4. Geological cross sections across the Yuechengling Massif. Locations are indicated in Figure 3. Rock symbols are the same in Figure 3. These sections show the tectonic units and their relationships with the Ziyuan Detachment. In the cross section C–C′, an insert of the petrological units displays a close view of the detachment. From up to bottom, four units of tectonites are distinguished: tectonic breccia, silicified cataclasite, mylonitic granite, and granite with shear bands and weakly oriented feldspar.

Yuechengling pluton (EYP) and the Western Yuechengling pluton (WYP; Figure 3). Close to the detachment, the granite is strongly mylonitized with shallow-dipping foliation, and stretching and mineral lineation (Figures 6a). The mylonitic foliation dips at a low angle (0–30°) to the west or WNW, but some of foliation that dips to SE may result from undulation of the detachment plane (Figures 4b–4d). Macroscopically, the foliation consists of alternation of biotite-rich matrix and light-colored, quartzofeldspathic interlayers (Figure 6a). On the foliation plane, lineation is marked by aligned biotite flakes and elongated quartz and feldspar grains or aggregates, showing a roughly WNW-ESE trending and shallow dip angles (Figure 6b). In some deformed rocks far from the ZYD, a NNE-SSW lineation shows a perpendicular direction to the regional lineation (Figure 3d). It can be a relict structure of Early Paleozoic synmagmatic deformation or related to pre-Cretaceous compressional events.

The intensity of deformation can be indicated by well-developed shear bands in the pluton. In high-strain rocks, the foliation is defined by the orientation of coarse feldspar and quartz grains, whereas the shear plane corresponds to segregation of biotite flakes. Close to the detachment, high-density shear bands are parallel to the foliation (Figure 6a). The angle between shear bands and foliation gradually decreases when the rocks evolved from orthogneiss to mylonite (Figures 6c and 6d). In the eastern part of the WYP, shear bands
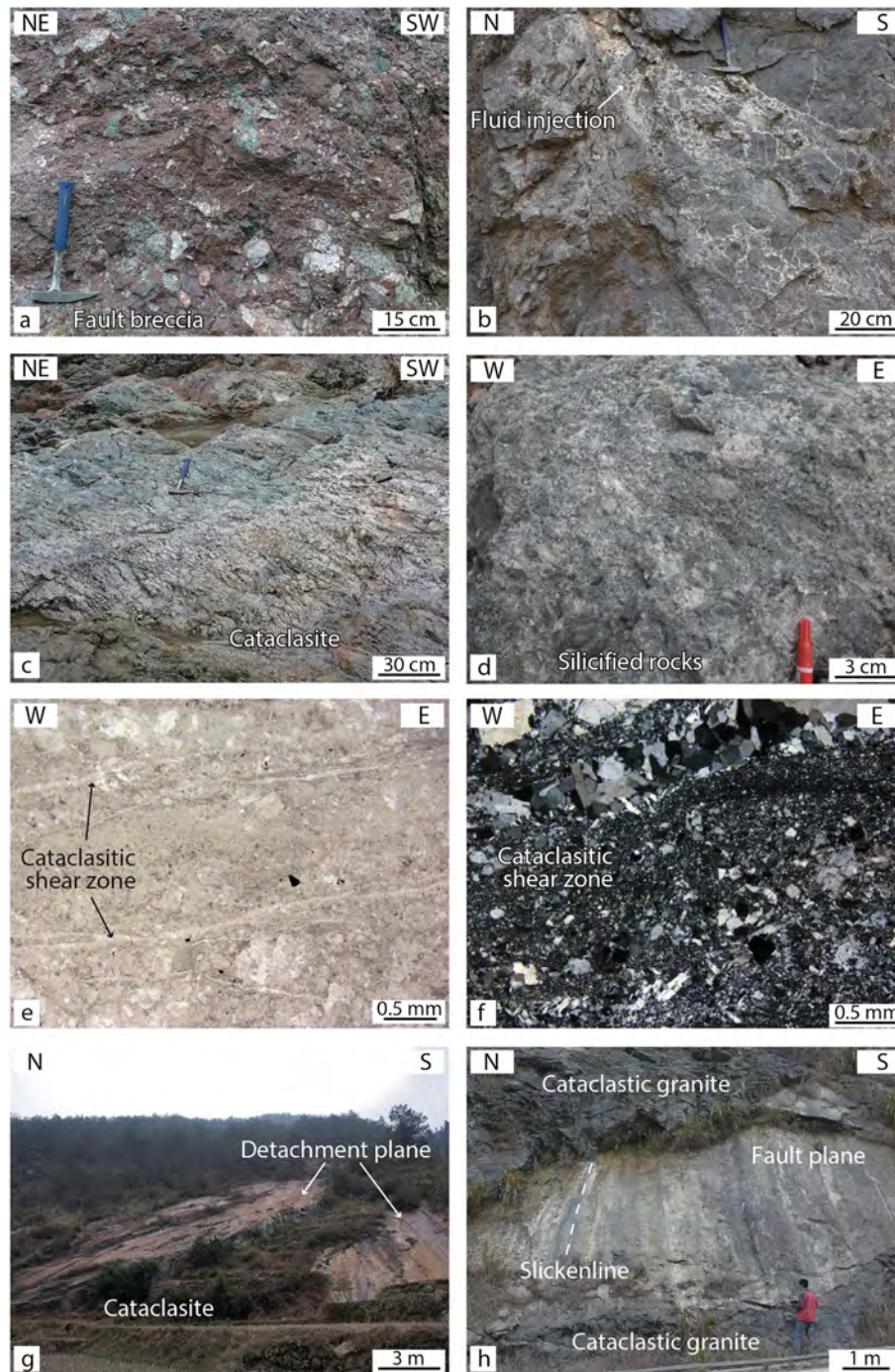
Figure 5. Field and microscopic photographs illustrating the deformation above the Yuechengling Detachment. (a) Fault breccia as the uppermost tectonite of the YCL Detachment, south of Meixi. Note that some granitic pebbles suggest the subaerial exposure of the Yuechengling pluton; the red pelitic matrix is compositionally similar to the Cretaceous sediments. (b) Faulted rocks with fluid activity, northeast of Xinning. Carbonated fluid is injected along faults or fissures. (c) Cataclasite of quartzite above the detachment, south of Meixi. All the rocks experienced brittle deformation and are full of cracks and faults. (d) Close view of silicified fault breccia, northeast of Ziyuan. Both the pebble and matrix are modified by silica-rich fluid. (e) Photomicrograph of cataclasite in which some brittle shear zones reduced the grain size by mechanical crushing, northeast of Meixi. (f) Deformed quartzite within a cataclastic shear zone, northeast of Meixi. Quartz grains with undulose extinction in the lower part show some ductile deformation. The cataclastic shear zone in the central part is filled with fragments of quartz at the expense of plastically deformed quartzite. (g) Fault plane of the Ziyuan Detachment, south of Meixi. This plane develops along the western boundary of the Yuechengling pluton with consistent westward dip with an average angle of 30°. (h) Fault planes developed in the granite, south of Xinning. Secondary fault of the Ziyuan Detachment partly cuts through the granite. Downdip slickenlines on the fault plane indicate top-to-the west normal faulting.
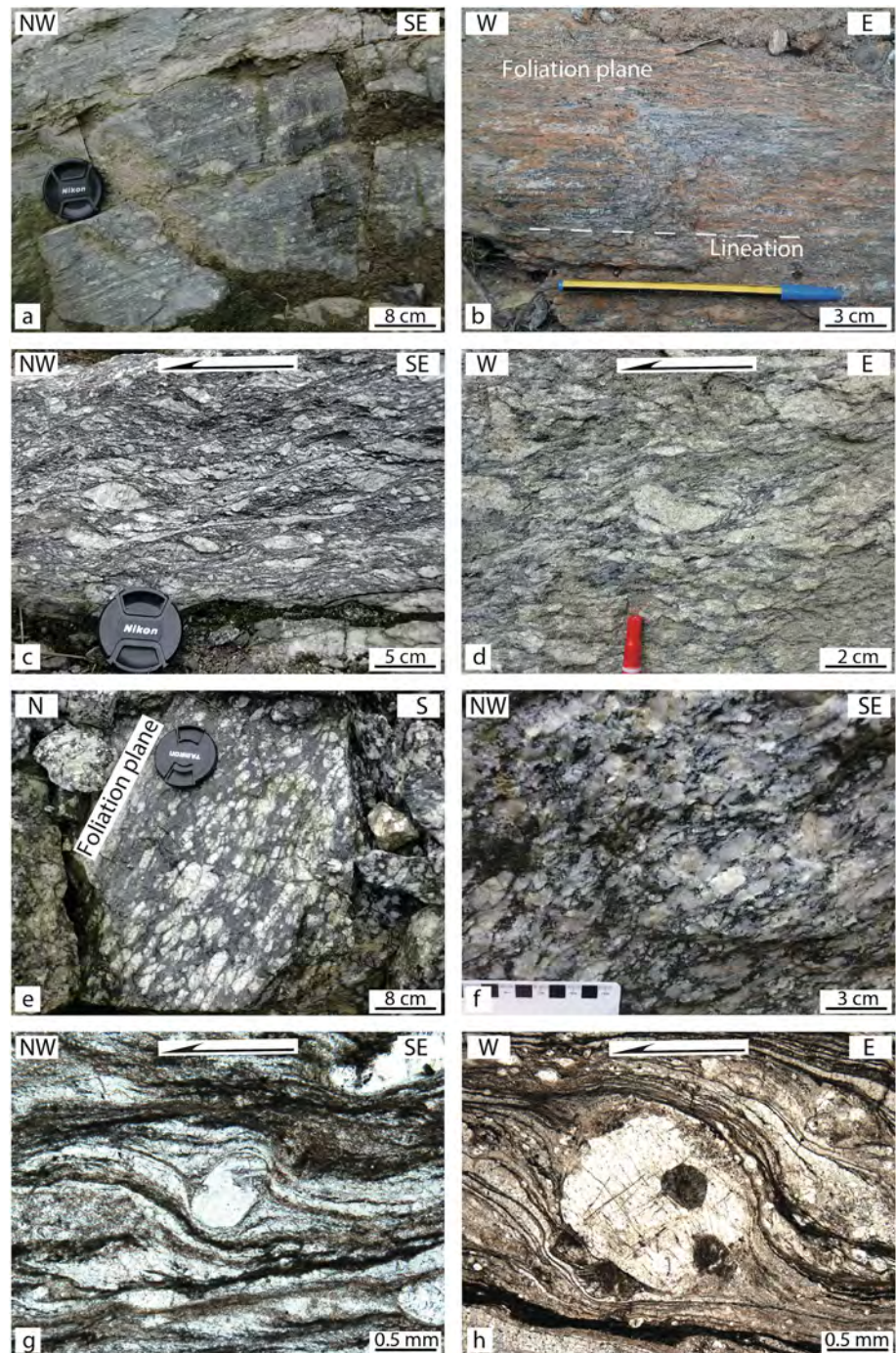
Figure 6. Field and microscopic photographs of mylonitic granite in the footwall of the Ziyuan Detachment. (a) NW dipping foliation of the mylonitic granite, south of Meixi. The foliated rock contains mica-rich layers and quartzofeldspathic layers. Sigmoidal feldspar porphyroclasts show a top-to-the NW shear sense. (b) E-W trending lineation on the foliation plane, east of Xinning. The lineation is composed of biotite and elongated quartz and feldspar aggregates. (c) Shear band structures in mylonitic granite, east-northeast of Ziyuan. The gently west dipping shear planes and the upper left-lower right foliation planes indicate a top-to-the NW sense of shear. (d) Sigma-type K-feldspar porphyroclasts that suggest a top-to-the west shear sense, southeast of Xinning. Note that the K-feldspar also experienced ductile deformation, implying a deformation temperature over 500 °C. (e) Preferred orientation of K-feldspar that forms mineral lineation on the foliation plane, northeast of Ziyuan. (f) Fabrics on the section parallel to the lineation and perpendicular to the foliation, South of Ziyuan. In this rock, shear sense is difficult to observe. (g) Delta-type plagioclase porphyroclasts with a top-to-the NW sense of shear in the mylonitic granite, southeast of Meixi. (h) Mylonitic granite with sigma-shape porphyroclasts of K-feldspar indicating a top-to-the west sense of shear, southeast of Meixi.

disappear in granites, but coarse feldspar grains are still oriented by consistent ductile shearing of extension, trending roughly E-W (Figure 6e). Most of feldspar grains have euhedral rectangular shape and smooth boundaries, as indicative that no recrystallization occurs at grain boundaries (Figure 6f).

Kinematic indicators document a consistent top-to-the west shear sense in the WYP. Sigma-shape structures in orthogneiss and shear bands preserved in mylonite both show top-to-the west shearing (Figures 6c and 6d). Photomicrographs show that strong mylonitization reduce mica and quartz grain size to form the dark matrix that surrounds the feldspar porphyroclasts. Delta- and sigma-type structures demonstrate a top-to-the NW/W shear sense (Figures 6g and 6h).

4.2.2. Deformation in the Tianhu Fault and EYP

The Tianhu Fault is a subvertical shear zone developed in the YCL pluton. Compared with the WYP, the foliation of the Tianhu Fault is subvertical or at a high angle with downdip lineation (Figures 3c and 3d). In this shear zone, the granite experienced high strain with a gneissic structure, in which the lineation is marked by alignment of quartz fibers and elongated feldspar grains (Figure 7a). Sheared feldspar porphyroclasts and asymmetrical pressure shadows display a top-to-the west shear sense during the normal faulting (Figure 7b). Bounded by the THF in the west, the EYP contains a narrow deformed zone in the vicinity of this normal fault, but the major part of the EYP yields isotropic textures (Figures 4a–4c). Most deformed rocks underwent a second phase of chloritization, which was caused by fluid injection and water-rock interaction along the shear planes. At the microscopic scale, we observe a combination of medium- and low-temperature deformation, in which feldspar grains are fractured and rotated, but polycrystalline quartz ribbons with equally sized grains show bulging and subgrain rotation. High-strain shear zones with a sharp contact to quartz bands suggest a cataclastic process resulting from low-temperature deformation, or likely linked to the later chloritization (Figure 7c). Large K-feldspar porphyroclasts with a domino structure argue for a top-to-the west shear sense (Figure 7d).

4.2.3. Deformation in the Neoproterozoic-Paleozoic Rocks

To the north and south of the YCL pluton, the Early Paleozoic sedimentary rocks intruded by the pluton have also been deformed by the ZYD, but the ductile deformation gradually weakens away from the detachment, and brittle structures dominate. Instead of mylonitic foliation, cleavage is prevalent in these rocks because of low-temperature deformation; nevertheless, the low dip angle to the west remains consistent in the entire area involved in the detachment (Figure 8a). As the deformation temperature decreases, folds become predominant in this upper crust section. Small detachment folds spread along pelitic zones in the Cambrian siltstone when strata are tilted (Figure 8b); recumbent folds with axial planar cleavage are produced by intense extensional shearing assisted by gravitational collapse (Figure 8c). Extensional structures can be followed along the ZYD northeasterly, whereas to the southwest, deformation disappears and the detachment terminates in the Late Paleozoic rocks (Figure 3a). Stretching lineation is uncommon in the metasedimentary rocks. To the east of the EYP, the exhumation of the YCL pluton generated a series of folds (Figure 8d). Along the contact between the granite and sedimentary rocks, rheological contrast facilitates the formation of layer-parallel slip and folding.

4.3. Hanging Wall of the Ziyuan Detachment

4.3.1. Cretaceous Xinning Basin

The synextension Xinning Basin locates immediately to the west of the ZYD (Figure 3a). This basin received a large amount of detritus from the footwall country rocks, including the YCL granite and Paleozoic sedimentary rocks. Two sedimentary units can be distinguished. The lower unit contains several hundred meters of purplish red thick-layered conglomerate with pebbles (<50 cm in diameter) and minor mudstone. The upper unit consists of 150-m-thick red conglomerate with pebbles around 1 cm in diameter (BGMRHN, 1988).

Separated from the detachment by a narrow zone of tectonic breccia or cataclasite, the base of this basin contains several hundred meters to a kilometer-thick conglomerate with angular to round pebbles within red pelitic matrix (Figure 9a). Near the detachment, unsorted pebbles show weakly developed bedding indicative of fast sedimentation by flood or landslide events. Upward, the stable sedimentation is characterized by conglomerate layers with round or elliptical pebbles. Based on rough counting of the rock types of pebbles, we find an along-strike correlation between sedimentation and erosion in this basin. In the north of this basin, most pebbles are limestone and dolomite that were likely derived from Carboniferous to Permian
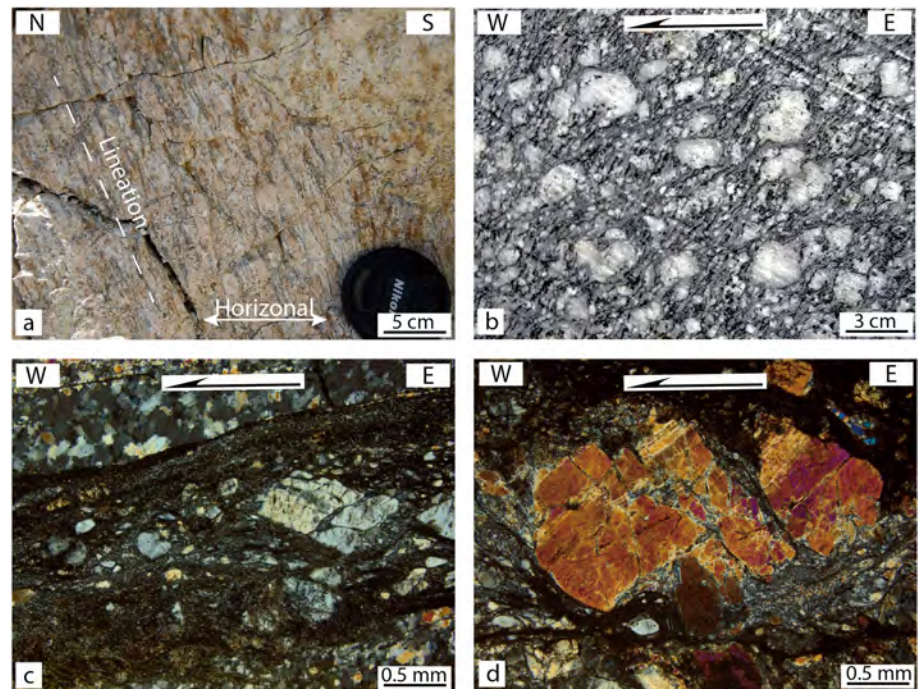
Figure 7. Field and microscopic photographs of the Tianhu Fault. (a) Subvertical foliation with downdip lineation formed by the alignment of quartz and K-feldspar, west-southwest of Daxijiang. Alteration with chloritization is also observed as a later overprint of the second stage of deformation. (b) Deformation fabrics on the plane parallel to the lineation and perpendicular to the foliation, north of Shanchuan. K-feldspar porphyroclasts show a top-to-the west shear sense. (c) Microscopic view of low-grade mylonitic granite, north of Shanchuan. Note the sharp boundary between the upper quartz band and lower cataclastic shear zone. The upper part consists of dynamically recrystallized quartz indicating a low deformation temperature at ca. 300 °C during the first stage. The cataclastic shear zone that deforms and cuts the previous structure indicates subsurface brittle deformation as an overprinting structure of the second stage. (d) K-feldspar porphyroclast with a book-shelf structure suggesting top-to-the west kinematics, northwest of Shanchuan. In contrast with the ductile deformation in quartz, the K-feldspar in the center is fractured into three major fragments in a domino type.

formations; southward, more and more granitic pebbles appear together with Early Paleozoic slate or metasandstone. Such a trend reveals uneven exhumation of the footwall. The middle and southern parts were more elevated and the deeper ductilely deformed unit experienced more erosion. In contrast, the northern part was less exposed and eroded, and thus, the contact between the weakly deformed Paleozoic pluton and country rocks at a shallow level is still preserved. Deformation is weak in the Cretaceous basin where most of the structures are conjugate joints and normal faults (Figure 9b).

4.3.2. Paleozoic Rocks

In the northern part of the hanging wall, Late Paleozoic limestone is juxtaposed with Early Paleozoic metasedimentary rocks by the ZYD. Brittle extension induced numerous normal faults in the Devonian to Permian limestone. Most fault planes dip at high angles (60–90°) to the west or east and throws along faults vary from 1 to 5 m (Figures 9c and 9d). Between two limestone layers, carbonated fluid circulated and crystallized along the slip plane, and the growth direction of calcite fiber indicates the layer-parallel slip motion (Figure 9e).

Early Paleozoic rocks occupy the major portion of the hanging wall in the south part of the study area. Compared with the northern part, extensional brittle structures are less widespread but still overprint on early structures. Metamorphosed rocks in a Triassic decollement zone are offset by a normal fault with a 1-m throw (Figure 9f). In this region, faults strike from NNW to NNE and generally dip to west or east. Folds are locally developed because of the weak effect of the extensional tectonics. The lower-grade metamorphism in the Early Paleozoic rocks of the north and south hanging wall suggests that the temperature of ductile deformation reached its maximum in the middle part and decreased northward and southward.
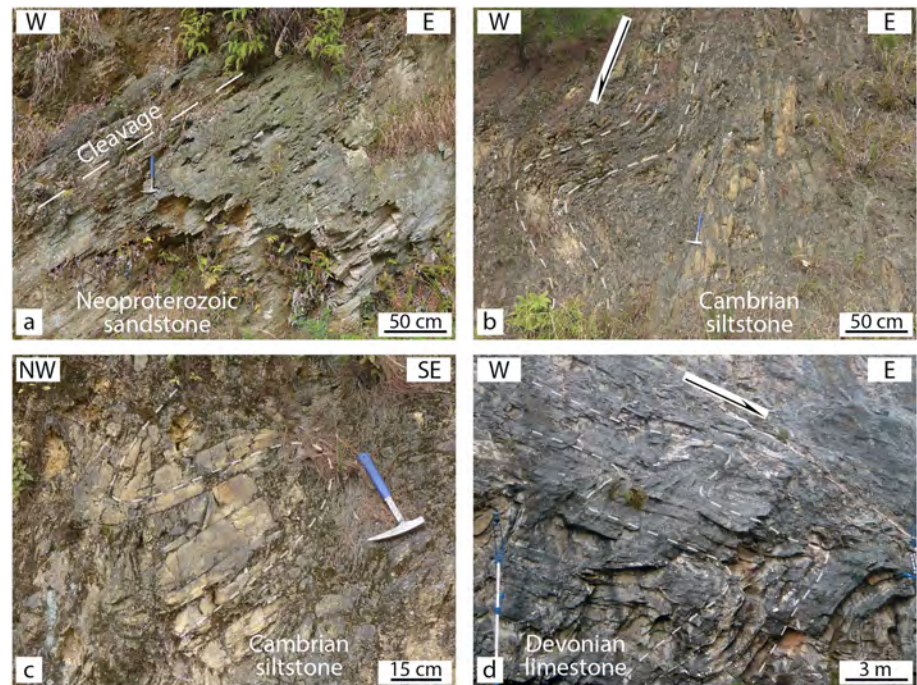
Figure 8. Field photographs of metasedimentary rocks in the footwall. (a) Strongly deformed Neoproterozoic sandstone with closely spaced cleavage, northeast of Xinning. The occurrence of the cleavage is consistent with the mylonitic foliation in the deformed granite as a result of detachment. (b) Detachment folds in Cambrian siltstone, northeast of Xinning. (c) Recumbent fold developed in Cambrian siltstone, east of Xinning. (d) Folds in Devonian limestone, indicating top-to-the east movement, west of Quanzhou.

5. Estimates of Deformation Temperature From Microstructures

In addition to regional- and outcrop-scale structural observation on the ZYD, dynamic recrystallization microstructures of quartz and feldspar are also analyzed in the sheared granites, aiming to decipher deformation mechanisms and temperature conditions (Figure 10).

In the vicinity of the detachment, samples of mylonitic granite exhibit deformation segregation in quartz grains. Ribbons at width of 3–5 mm consist of large quartz aggregates with undulose extinction. These quartz grains show varied sizes from 50 to 500 μm in diameter, but they have all undergone elongation with irregular boundaries (Figure 11a). Amoeboid grains with large-amplitude sutures indicate that grain boundary migration played an important role in accommodating the ductile shearing. Hence, we can infer that the deformation temperature is approximately 450 to 550 °C (Stipp et al., 2002). Another type of quartz grains is also observed in our samples. Within quartz-rich zones, some grains with long axes oblique to the foliation are highly elongated with length-width ratios larger than 10:1. Recrystallized grains also show undulose extinction (Figure 11b). In some shear zones, quartz is further sheared and recrystallized into smaller grains less than 10 μm in diameter. These fabrics with equigranular quartz neoblasts are characteristic of subgrain rotation recrystallization, indicating deformation temperature at 400–500 °C (Law, 2014; Stipp et al., 2002). In contrast to dynamic recrystallization in quartz, deformation in feldspar grains is accommodated by brittle fracturing; shear zones surround the feldspar because of its high stiffness (Figure 11c). Bulging recrystallization is rare at edges of feldspar grains, and core-and-mantle structures are absent. Under medium temperature (<500 °C), deformation in feldspar is still dominated by internal microfracturing and minor dislocation glide (Passchier & Trouw, 2005). Considering all the textures discussed above, the mylonitic granites in the YCL pluton yield an estimated deformation temperature from 400 to 500 °C.

Beneath the mylonite, the gneissic granites contain large undeformed feldspar grains, in which fractures showing no offset are filled with tiny quartz grains (Figure 11d). At rims of feldspar grains, deformation twinning results from the stress concentration at the bulging points, but dynamic recrystallization is still absent. Large quartz grains show undulose extinction and bulging recrystallization in the cores and rims,

Figure 9. Photos of deformation features in the hanging wall. (a) Cretaceous conglomerate in which 90% of pebbles are limestone, northeast of Xinning. The variable size and angular shape of pebbles testify to rapid deposition in a fault-controlled alluvial fan. (b) X-shape joints developed in Cretaceous red sandstone, northeast of Meixi. The conjugated joints suggest horizontal extension (E-W) that is consistent with the regional extensional regime. (c) Normal faulting in Devonian limestone, northeast of Xinning. (d) A normal fault in Devonian sandstone, showing a clear offset of a thick sandstone layer, northeast of Xinning. (e) E-W trending slickenlines and calcite steps on a normal fault plane that cuts Carboniferous limestone, north of Xinning. (f) Weakly metamorphosed Ordovician siltstone cut by a high-angle normal fault, north of Huajiang.

respectively. In some quartz grains, mechanical twinning occupying the entire area reflects a lower rigidity of quartz and also indicates a low deformation temperature at 250 to 350 °C (Passchier & Trouw, 2005). Shear zones separating large feldspar and quartz aggregates consist of fine grains of quartz and biotite assemblage, but the sharp boundary may suggest that these small grains were formed by grain-size reduction, rather than recrystallization, indicating a deformation temperature at ~300 °C (Figures 11d and 11e). To summarize, low-temperature deformation in the brittle-ductile transitional zone is the ruling mechanism during the extensional deformation of the gneissic granites.

Strongly sheared granites along the THF share similarities of deformation structure within the gneissic granites in the WYP. Quartz grains exhibit undulose extinction, and, along the grain boundaries, newly formed fine grains are created from the host grain by bulging recrystallization (Figure 11f). Strain localization gives rise to microscopic shear zones, in which grains are crushed and elongated; biotite is also sheared to mica fish structure. These fabrics are consistent with low-temperature deformation that occurs at 300 to 350 °C (Law, 2014; Passchier & Trouw, 2005).
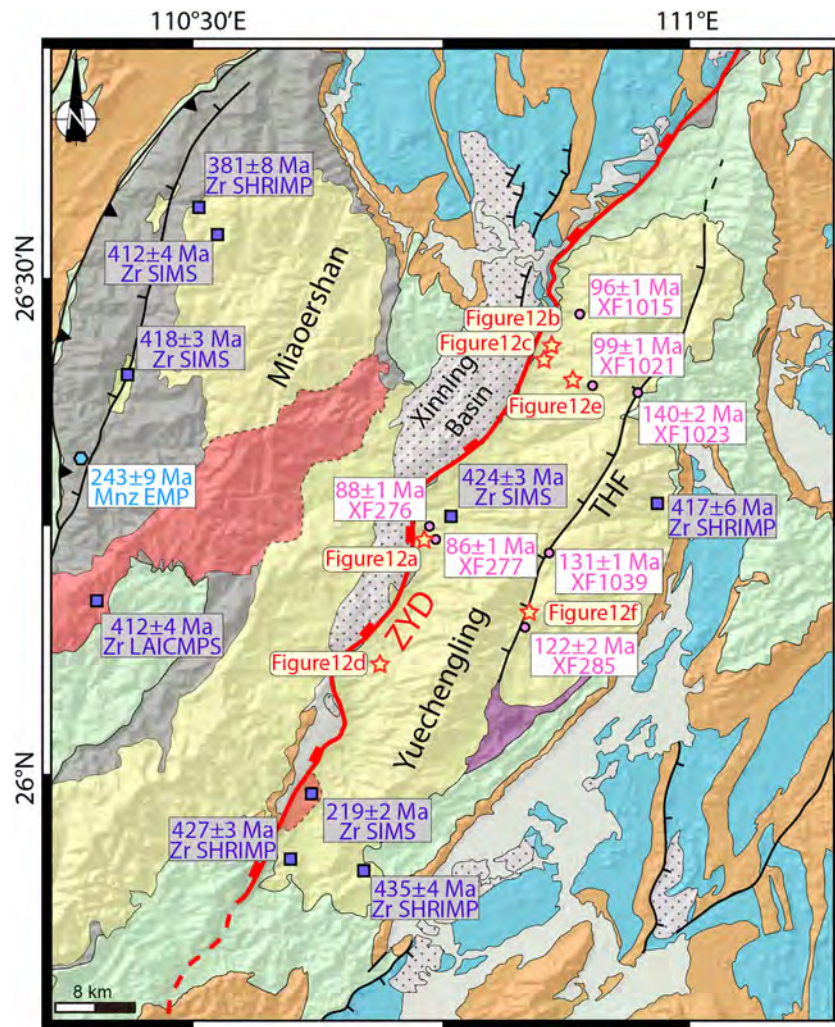
Figure 10. Age compilation of the Yuechengling Massif and its adjacent region. Symbols: Purple square: Zircon (Zr) U-Pb ages. Dating methods are also indicated with the age number (Zr SIMS data from Chu, Faure, Lin, Wang, & Ji, 2012, Chu, Lin, Faure, Wang, & Ji, 2012; Zr SHRIMP data from Zhao et al., 2013). Blue hexagon: Monazite (Mnz) U-Pb age by electron microprobe chemical dating (Data from Chu, Faure, Lin, Wang, & Ji, 2012). Orange circle: Ar-Ar age data in this study. Yellow star: Analyzed sample location for determination of deformation temperature.

To summarize, mylonitic granites experienced high-temperature deformation accommodated by quartz subgrain rotation and grain boundary migration transition at 400 to 500 °C; gneissic granites far from the detachment record low-temperature deformation between 300 and 350 °C, under which bulging recrystallization dominates in quartz deformation whereas feldspar displays brittle structures.

6. Geochronology

6.1. Analytical Method of ^{40}Ar-^{39}Ar Dating

Rock samples were cleaned and crushed, and biotite grains were then hand-picked under a binocular microscope. Before preparation for dating, we rechecked biotite to select fresh, clear crystals without inclusions, impurities, or alteration. Detailed analytical procedure was described by Wang et al. (2009). High-resolution ^{40}Ar/^{39}Ar measurements were performed by using mass spectrometer MM5400 at ^{40}Ar/^{39}Ar and U-Th/He laboratory in the Institute of Geology and Geophysics, Chinese Academy of Sciences (IGGCAS), Beijing. Analytical data were processed using the excel-based software-ArArCALC (Koppers, 2002), and external uncertainties from procedures were also included and propagated into the final results. Errors are reported at the 2-sigma confidence level.
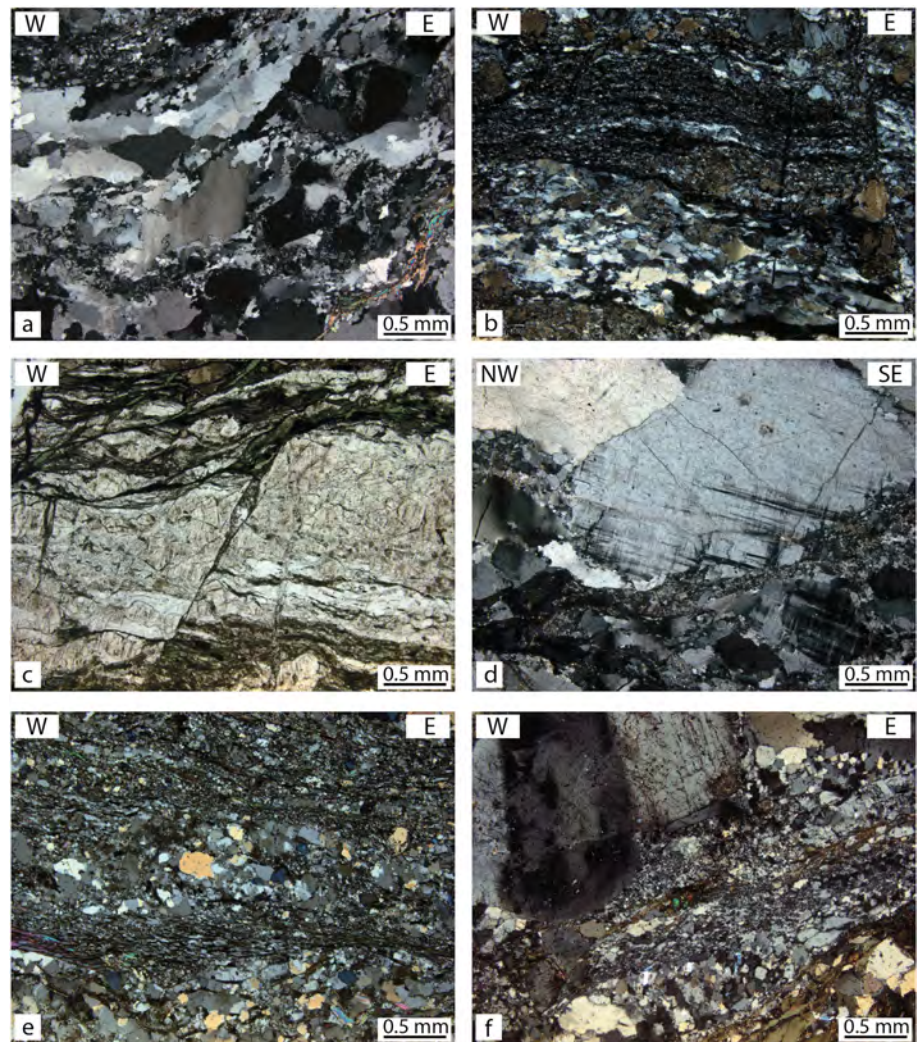
Figure 11. Photomicrographs of selected samples for temperature estimation in the Yuechengling Massif. Location is indicated in Figure 10. (a) Polycrystalline quartz ribbons at width of 3–5 mm. Large quartz aggregates with irregular boundaries and undulose extinction. Amoeboid grains indicate grain boundary migration that occurred at a deformation temperature of 450 to 550 °C. (b) Highly elongated quartz grains with oblique shape fabric with respect to the foliation. Note that some recrystallized grains with length-width ratios larger than 10:1 exhibit undulose extinction zones. These fabrics with equigranular quartz neoblasts suggest subgrain rotation recrystallization at 450–550 °C. (c) Brittle fracturing with book-shelf structures in K-feldspar. Shear zones develop around the feldspar because of its high stiffness but localized bulging recrystallization occurs at the K-feldspar boundary. (d) Gneissic granites that contain large undeformed feldspar grains with fractures filled with tiny quartz grains. At rims of feldspar, deformation twinning result from stress concentration on bulging points without dynamic recrystallization. (e) Shear zones separating bands of large feldspar/quartz aggregates. The sharp boundary suggests grain-size reduction rather than recrystallization as a result of low-temperature deformation. (f) Strongly sheared granite in the Tianhu Fault. Quartz grains exhibit undulose extinction and bulging recrystallization. Microscopic shear zones have crushed and elongated grains; biotite is sheared to mica fish, which are consistent with low-temperature deformation at 300 to 350 °C.

6.2. ^{40}Ar-^{39}Ar Dating Results

Detailed biotite ^{40}Ar/^{39}Ar analytical results, sampling coordinates, and mineralogy of seven samples are listed in Table 1 and Data Sets S1–S3 in the supporting information. Information of locations and ages is also marked in Figure 10. Four samples from the ZYD were gathered from the WYP. Three samples were collected along the THF. All of the samples present well-resolved plateaus comprising 60–100% of the total ^{39}Ar(K) released. In order to better understand the obtained ages, inverse isochrons and age plateaus are presented in Figures 12 and 13.

Table 1
Detailed Information of Selected Samples for ^{40}Ar-^{39}Ar Dating

Sample No.	Latitude (°N)	Longitude (°E)	Rock type	Quartz recrytallization	Estimate on deformation temperature (°C)	Mineral	Method	Age (Ma)	2σ (Ma)
XF276	26.15923	110.73142	Mylonitic granite	GBM + SGR	450–500	Biotite	Plateau	88.2	0.5
XF277	26.15363	110.73318	Mylonitic granite	GBM + SGR	450–500	Biotite	Plateau	86.6	0.5
XF1015	26.38314	110.88126	Mylonitic granite	GBM + SGR	450–500	Biotite	Plateau	96	1.1
XF1021	26.30051	110.89328	Gneissic granite	GBM + SGR	450–500	Biotite	Plateau	99	1.1
XF285	26.0745	110.83115	Gneissic granite	BLG + SGR	350–400	Biotite	Plateau	121.9	5.7
XF1023	26.2964	110.93224	Gneissic granite	BLG	300–350	Biotite	Plateau	139.7	1.6
XF1039	26.13393	110.84855	Gneissic granite	BLG	300–350	Biotite	Plateau	131.4	1.4

Note. GBM: grain boundary migration; SGR: subgrain rotation; BLG: buldging recrystallization.

Samples XF276 and XF277, collected in the detachment, yield flat age spectra at 88.2 ± 0.5 and 88.6 ± 0.5 Ma, accounting for 95% and 100% of released ^{39}Ar, respectively (Figures 12a and 12b). The initial $(^{40}Ar/^{36}Ar)_0$ ratios of 303.8 and 298.6 show slight excess Ar, but their inverse isochron ages are similar within error, indicating negligible effect on ages.

Samples XF1015 and XF1021 are gneissic granites structurally located beneath the mylonitic granites. Two plateaus both contain steps with >98% of released ^{39}Ar, yielding ages at 96.0 ± 1.1 and 99.0 ± 1.1 Ma, respectively. Despite excess Ar in XF1015, the isochron age is consistent with the plateau age and the total fusion age, so the age at 96 Ma is reliable for further discussion. XF1021 does not exhibit excess Ar component.

Samples XF285, XF1023, and XF1039 from the THF show more complicated age spectra. A weighted plateau age of XF285 is calculated at 121.9 ± 5.7 Ma with the highest error in all analyzed samples, partly because only three stages with 60% of released ^{39}Ar are calculated (Figure 13a). The total fusion age (122.7 ± 2.4 Ma) and the inverse isochron age (120.3 ± 10.3 Ma) are similar to the plateau age within error. The uneven pattern of the age spectra is likely linked to late activity and chloritization of this fault, which is supported by a younger spectrum ages at ~100 Ma (Figure 13a). In contrast, the other two samples (XF1023 and XF1039) yield flat age spectra accounting for 70% and 90% of the released ^{39}Ar, respectively. XF1023 has a plateau age at 139.7 ± 1.6 Ma, same as the inverse isochron age and the total fusion age, which does not show any influence by excess Ar (Figure 13b). Consistent ages are obtained in XF1039 by weighted plateau, total fusion, and inverse isochron, so the weighted plateau age with 90% of released ^{39}Ar at 131.4 ± 1.4 Ma is preferred here to account for the cooling age of this sample (Figure 13c).

7. Discussion

### 7.1. Deformation History of the Yuechengling Massif

Together with microstructural and ^{40}Ar-^{39}Ar data, our new field observations allow us to draw a Cretaceous tectonic scenario from the evolution of the YCL Massif. As the major structure in the study region, the Ziyuan Detachment developed extensive ductile and brittle deformation that affected the adjacent pluton and the Xinning Basin (Figures 3, 4, and 14). The footwall and the hanging wall of the ZYD show different deformation features. The structural fabrics in the footwall rocks comprise consistent NNE striking foliation and west trending stretching and mineral lineation. Furthermore, the THF divides the YCL pluton into the EYP and the WYP with distinct deformation patterns. The entire WYP is involved into ductile shearing, resulting in mylonites or gneissic granites that share a similar top-to-the west shear sense. In the EYP, the deformation is localized in the vicinity of the THF, and most part of the EYP is isotropic. The hanging wall merely records brittle faults and joints that cut the Triassic compressional structures (Chu, Faure, Lin, Wang,
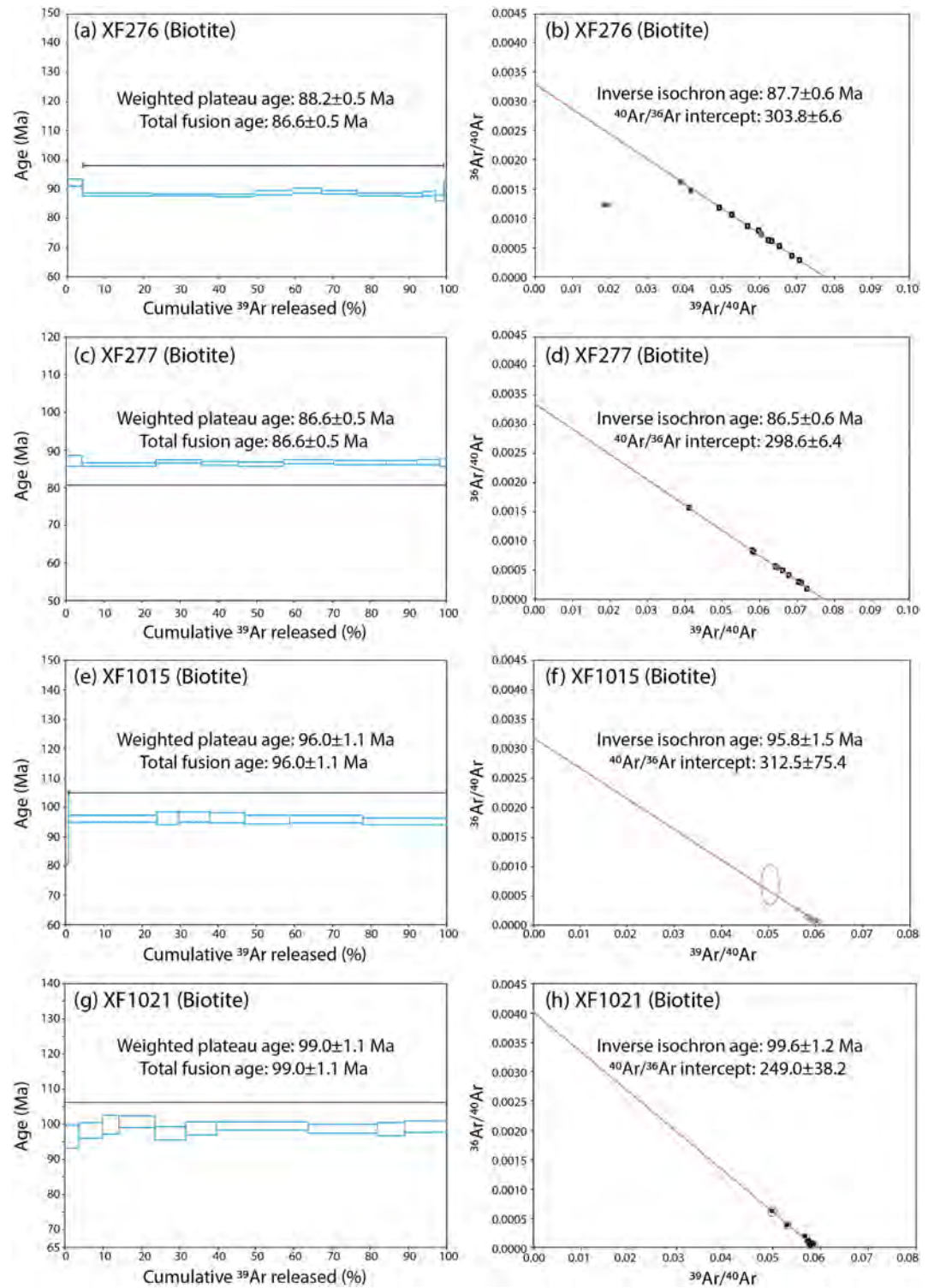
**Figure 12.** Diagrams of ^{40}Ar-^{39}Ar dating results in the Western Yuechengling pluton. Age spectra and inverse isochrons are shown in (a and b) XF276, (c and d) XF277, (e and f) XF1015, and (g and h) XF1021. Sample location is marked in Figure 10.
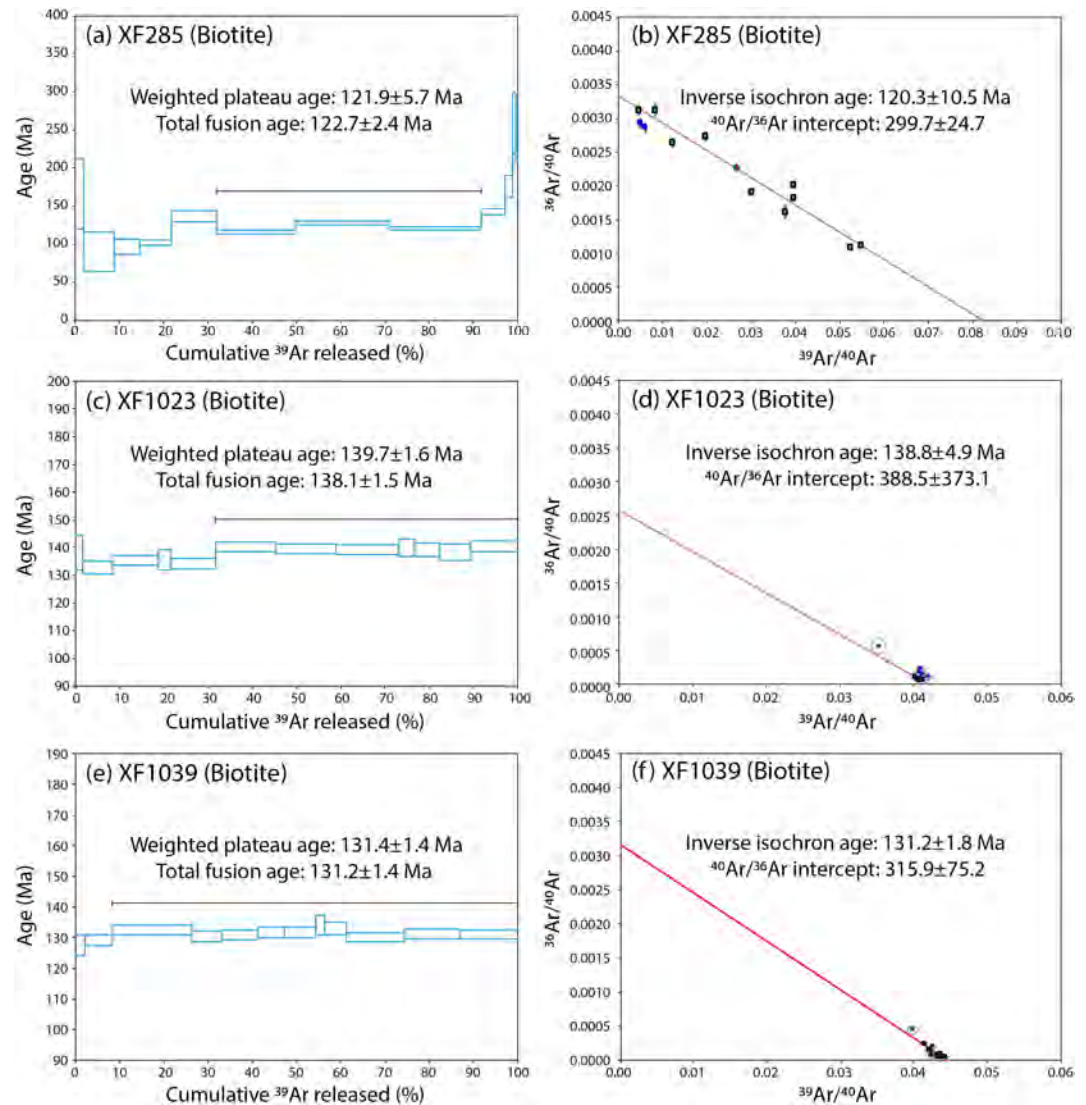
Figure 13. Diagrams of ^{40}Ar-^{39}Ar dating results in the Eastern Yuechengling pluton. Age spectra and inverse isochrons are presented in (a and b) XF285, (c and d) XF1023, and (e and f) XF1039. Sample location is marked in Figure 10.

& Ji, 2012). Extension-related folds are widespread in sedimentary rocks across the whole region. Based on our geometrical and kinematic analysis, the YCL Massif is therefore a typical extensional dome controlled by the ZYD.

Our new ^{40}Ar-^{39}Ar dating results on biotite of mylonitic and gneissic granites provide precise constraints on the deformation sequence in the YCL Massif. Three samples collected from the Tianhu Fault yield ^{40}Ar-^{39}Ar ages between 140 and 120 Ma, interpreted to be the timing of the early D_1 extensional event. D_1 developed a narrow shear zone in the middle of the YCL pluton, exhumed the footwall EYP, and produced extensional structures, such as folds and conjugate joints, in the Paleozoic to Mesozoic strata (Figure 14a). The ductile deformation is restricted to the THF, triggering low-temperature mylonitization dominated by shear bands and bulging recrystallization of quartz, and brittle fracturing of feldspar at microscopic scale. Whether syn-tectonic basins along the THF existed during D_1 remains ambiguous, because the exposures have been erased by later uplifting of the WYP. However, despite the lack of evidence of D_1 deformation, the Early Cretaceous sedimentary record in the Xinning Basin may indicate that the initiation of the ZYD was coeval with the activity of the THF (BGMRHN, 1988). According to our Ar-Ar results, the WYP was still buried at depth >10 km, and the dominant limestone pebbles in basal conglomerate of the Xinning Basin hint that the Paleozoic cover was overlying the YCL pluton (Figure 14a).
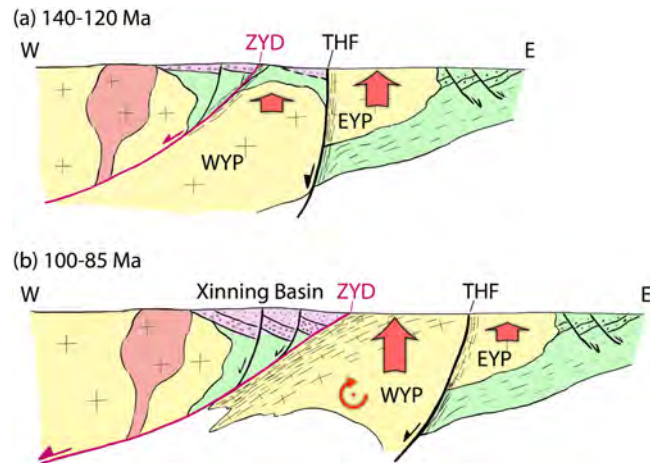
Figure 14. Schematic evolution models of the Yuechengling Massif. (a) First stage (140–120 Ma): The Tianhu Fault (THF) was active with a narrow mylonitic zone and exhumed the Eastern Yuchengling pluton (EYP). The Ziyuan Detachment (ZYD) showed limited exhumation. (b) Second stage (100–85 Ma): The Ziyuan Detachment accommodated most of crustal stretching. The Western Yuechengling pluton (WYP) was intensively deformed, clockwise rotated, and exhumed. The Tianhu Fault was partly reactivated with subsurface alteration with a small amount of uplifting.

The activity of the ZYD that occurred at 100–85 Ma, as revealed by four new ages in the WYP, accounts for the final geometry of this region. The entire WYP underwent extensive ductile deformation with pervasive mylonitic or gneissic foliation and consistent stretching and mineral lineation, indicating a top-to-the west shear sense. We ascribe this deformation to the D_2 event responsible for the major exhumation of the YCL Massif. Mylonitic fabrics show a different mechanism from that of D_1. Microstructure in quartz and feldspar grains suggests high-temperature deformation at ~500 °C, intimately connected to a high thermal state in the South China crust during the Late Cretaceous. The gneissic granites exhibit low-temperature fabrics at 300–350 °C as indicated by quartz bulging recrystallization. Since the deformation temperature of the gneissic granite is close to the closure temperature for biotite Ar-Ar dating, the age at 99 Ma of sample XF1021 can be assumed as the onset of the D_2 event. Although the D_2 ductile deformation is not recorded in the EYP and the THF, fluid activity and resultant chloritization along the fault plane may also trigger the subsurface reactivation, as suggested by steps and striations within the THF zone. This lower-temperature disturbance cannot be recorded by Ar-Ar dating because of the closure of Ar-diffusion system in biotite (Dodson, 1973).

Given the structural analysis and geochronological results, we argue that two stages of extension controlled the tectonic evolution of the YCL Massif (Figure 14). The early extension event, D_1, between 140 and 120 Ma, exhumed the EYP through the THF. A partial initiation of the ZYD Detachment can be traced by the Early Cretaceous sedimentation in the Xinning Basin, which indicates limited exhumation of the WYP and its neighboring areas (Figure 14a). The second stage of extension, D_2, lasted from 100 to 85 Ma and the major ductile shearing that deformed the YCL Massif. Due to the regional stretching, the surface increase was mostly accommodated by fast exhumation of middle crustal material, such as the WYP, which shows extensive medium- to high-temperature fabrics as evidence for its middle crust level during deformation (Figure 14b).

At these two stages, exhumation was accommodated in different deformation patterns. During the early phase of extension, the high-angle ductile THF was dominated by vertical exhumation of upper-middle crust rocks. The shallow structural level and limited exhumation may account for the high angle of this ductile fault zone. In contrast, in the late phase, the low-angle ZYD caused large-scale exhumation of middle-lower crustal rocks and the rotation of the WYP, consistent with the pattern of MCCs in western United States (Davis & Lister, 1988; Wernicke, 1981).

7.2. Cretaceous Episodic Extension in the SCB

The extensional tectonics and the voluminous Late Mesozoic magmatism of eastern Asia have been attributed to the oceanic subduction of the Paleo-Pacific/Izanagi plate (Ren et al., 1990; Zhou & Li, 2000). However, the process and temporal-spatial distribution of the extension, and its geodynamic mechanisms, still require refinement with further structural, geochronological, and petrological work. In comparison

with the NCB in which most of the extensional domes or MCCs appeared in the Early Cretaceous (Lin et al., 2008; Wang et al., 2014; Wang, Zheng, et al., 2011), the SCB presents a protracted extensional regime manifested by extensional domes and basins active from 140 to 80 Ma, but each of these domes seems to have a distinctive evolution history (Li et al., 2013, 2014; Lin et al., 2000; Shu et al., 2009; Zhou & Li, 2000; Zhu, Xie, et al., 2010).

Across the SCB, extensional domes or MCCs are only developed in the central region at least 400 km far from the plate boundary (Figure 15). In the southern part of this huge extensional province, as revealed by our new structural and geochronological data, the Yuechengling Massif experienced a two-stage extension (140–120 and 100–85 Ma) recorded in ductile deformed rocks. In fact, this episodic extension has also been recognized in other extensional structures. In the northern part of the SCB, the Tongbai and Dabie Massifs superimposed on the Triassic Qinling-Dabie orogenic belt both recorded Cretaceous extension and unroofing that accommodate the final exhumation of the lower crustal rocks (Cui et al., 2012; Hacker et al., 2000; Ji, Lin, Faure, Shi, et al., 2017; Ratschbacher et al., 2000; Webb et al., 1999; Xu & Wang, 2010). They share similar kinematics with top-to-the NW shearing but indicate different exhumation stories. Ar-Ar cooling ages of Tongbaishan (TBS) yield two stages of deformation at 140–115 and 105–85 Ma, whereas Dabieshan (DBS) shows a dominant age cluster at 140–115 Ma, suggesting that the Early Cretaceous deformation with contemporaneous migmatization and magmatism gave rise to almost all of the exposed rocks (Figure 16a). However, minor Late Cretaceous cooling ages correspond to later uplifting or thermal perturbation and can thus be linked with the Late Cretaceous extension (D_2 event; Webb et al., 1999; Ratschbacher et al., 2000; Ji, Lin, Faure, Shi, et al., 2017). At the northern margin of the SCB, the early extension seems to have a more widespread impact, because these extensional/magmatic domes, including the Huangling Massif (HL), Qingyang-Jiuhua plutons (QY-JH), and Hongzheng MCC (HZ), were formed during Early Cretaceous without later cooling ages (Ji et al., 2014; Wei, Martelet et al., 2014; Wei, Chen, et al., 2014; Zhu, Xie, et al., 2010).

In contrast to the northern region, the two-stage evolution model plays a more important role in those more southerly extensional domes (Figure 15), that is, Dayunshan (DYS), Lushan (LS), Hengshan (HS), and Yuechengling (YCL), and dictates different rock deformation patterns in response to the two events. The DYS and HS domes are both characterized by NW-SE stretching with a top-to-the NW shear sense, and the detachments were active between 140 and ~85 Ma (Ji et al., 2018; Ji, Faure, et al., 2018; Li et al., 2014, 2016). Although the possibility of a long-lived detachment cannot be excluded, the cooling age patterns exhibit a ~20-Myr interval between the two age peaks (Figure 16a), implying intermittent movement of the detachments. The YCL Massif preserves a consistent deformation pattern with two phases of ductile deformation and exhumation at 140–120 and 100–85 Ma, respectively. Comparably, the Lushan MCC shows two phases of deformation. The first one (~125 Ma) resulted in syntectonic granitic intrusion and NE-SW stretching, while the second one (~110–85 Ma) produced normal faults and red bed basins that account for the regional fast cooling (Lin et al., 2000; Zhu, Yang, et al., 2010).

Previous structural work provides detailed analysis and timing on these structures. All of these results, including our new data, allow us to illustrate a consistent tectonic scenario with episodic back-arc extension during the Paleo-Pacific subduction. Two age clusters are clearly displayed at 140–120 and 105–85 Ma, representing two stages of crustal extension and exhumation-cooling of lower crustal rocks (Figure 16b). The two magmatic pulses documented during the Cretaceous, at 140–120 and 105–85 Ma, fit well with the two stages of extension (Figures 16c and 16d). In central and eastern South China, numerous extensional basins also underpin the Cretaceous stretching of the lithosphere during the Cretaceous (Figure 15). NE trending basins developed along regional normal faults, and their sedimentary infill includes coeval volcanic or volcaniclastic rocks (BGMRJX, 1984; BGMRZJ, 1989; Shu et al., 2009). It is noteworthy that a regional unconformity between the Early and Late Cretaceous strata represents a pause between the two stages of the extensional tectonics (BGMRJX, 1984; BGMRZJ, 1989). In contrast to the early stage, large basins were mostly located in the central part of South China (Figure 15), which was regarded as the more extended region in agreement with the distribution of the extensional domes and MCCs (Ji, Faure, et al., 2018; Li et al., 2014; Lin & Wei, 2019; Shu et al., 2009).

As a unique place of the Cretaceous Paleo-Pacific subduction system in East Asia, the SCB shows two stages of back-arc extension in association with coeval magmatic flare-ups. Compared to the short period, that is, Early Cretaceous, of the extension in the NCB, the tectonic evolution recorded in the SCB reflects a cyclicity of a subduction system.
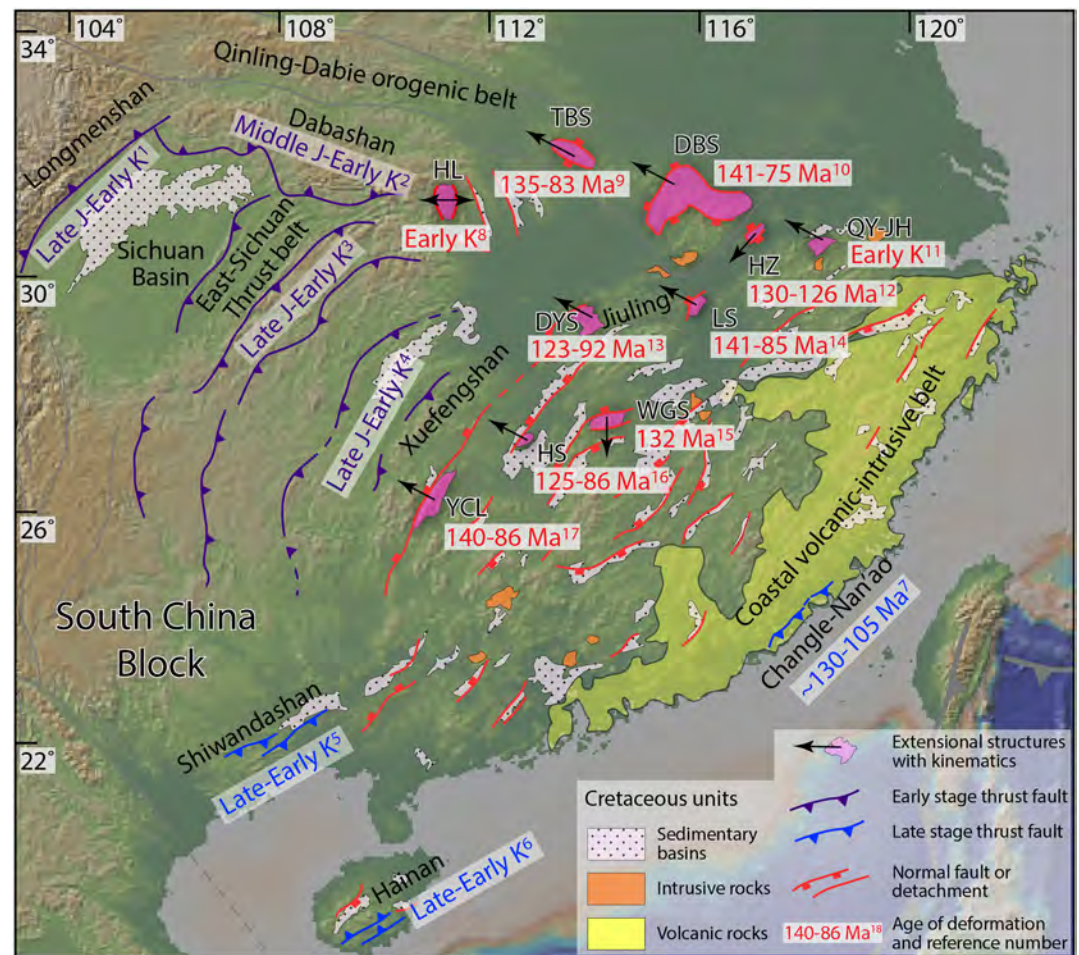
Figure 15. Tectonic map with localized Cretaceous deformation of the South China Block (SCB). Two stages of compression are recognized in the interior and margin of the SCB, respectively. The western part of the SCB is characterized by Late Jurassic-Early Cretaceous thrusting, and the eastern margin records Late-Early Cretaceous deformation. Between them, a large extensional province is expressed by numerous extensional structures active at 140–120 and 105–85 Ma. The intrusive rocks located in the coastal volcanic belts are not marked. References for the timing of different tectonic units are as follows: 1. Longmenshan (Xue et al., 2017; Yan et al., 2011); 2. Dabashan (Dong et al., 2013; Li et al., 2015); 3. East Sichuan Thrust Belt (Yan et al., 2003, 2009); 4. Xuefengshan (Li et al., 2012; Yan et al., 2003); 5. Shiwandashan (Liang & Li, 2005); 6. Hainan (Chen, 2013); 7. Changle-Nan'ao (Wei et al., 2015); 8. Huangling-HL (Ji et al., 2014); 9. Tongbaishan-TBS (Cui et al., 2012; Webb et al., 1999; Xu & Wang, 2010); 10. Dabieshan-DBS (Chen et al., 1992; Eide et al., 1994; Hacker & Wang, 1995; Hou et al., 2007; Ji, Lin, Faure, Shi, et al., 2017; Lin et al., 2007; Ratschbacher et al., 2000; Wang et al., 2011; Webb et al., 1999; Zhu et al., 2005); 11. Qingyang and Jiuhua-QY-JH (Wei, Chen, et al., 2014; Wei, Martelet, et al., 2014); 12. Hongzhen-HZ (Zhu, Xie, et al., 2010); 13. Dayunshan-DYS (Ji, Lin, Faure, Chen, et al., 2017; Ji, Faure, et al., 2018); 14. Lushan-LS (Lin et al., 2000; Liu et al., 2008; Wang et al., 2013; Yang et al., 2017; Zhu, Yang, et al., 2010); 15. Wugongshan-WGS (Faure et al., 1996; Lou et al., 2005); 16. Hengshan-HS (Li et al., 2013, 2016; Wang et al., 2015); 17. Yuechengling-YCL (Wu et al., 2012; this study).

7.3. Cretaceous Tectonic Cycles of the South China Continental Margin

The SCB witnessed two Cretaceous extensional events at ~140–120 and ~105–85 Ma, respectively, both of which were accompanied with voluminous volcanic eruptions and intrusions (Figures 16c and 16d). Before the Cretaceous, an earlier magmatic flare-up between 180 and 155 Ma is manifested by an outburst of intrusive rocks across the entire SCB (Zhou et al., 2006; Zhou & Li, 2000). Therefore, the three magmatic flare-ups are divided by two episodes of magmatic quiescence at the Jurassic-Cretaceous boundary and in the late Early Cretaceous (Li, 2000; Li et al., 2010). Coeval with these magmatic lulls, compressional deformation influenced both the margin and interior of the SCB around 155–140 and 120–105 Ma. Hence, the Late Jurassic to Late Cretaceous tectonic evolution of the SCB can be subdivided into two cycles at 155–120
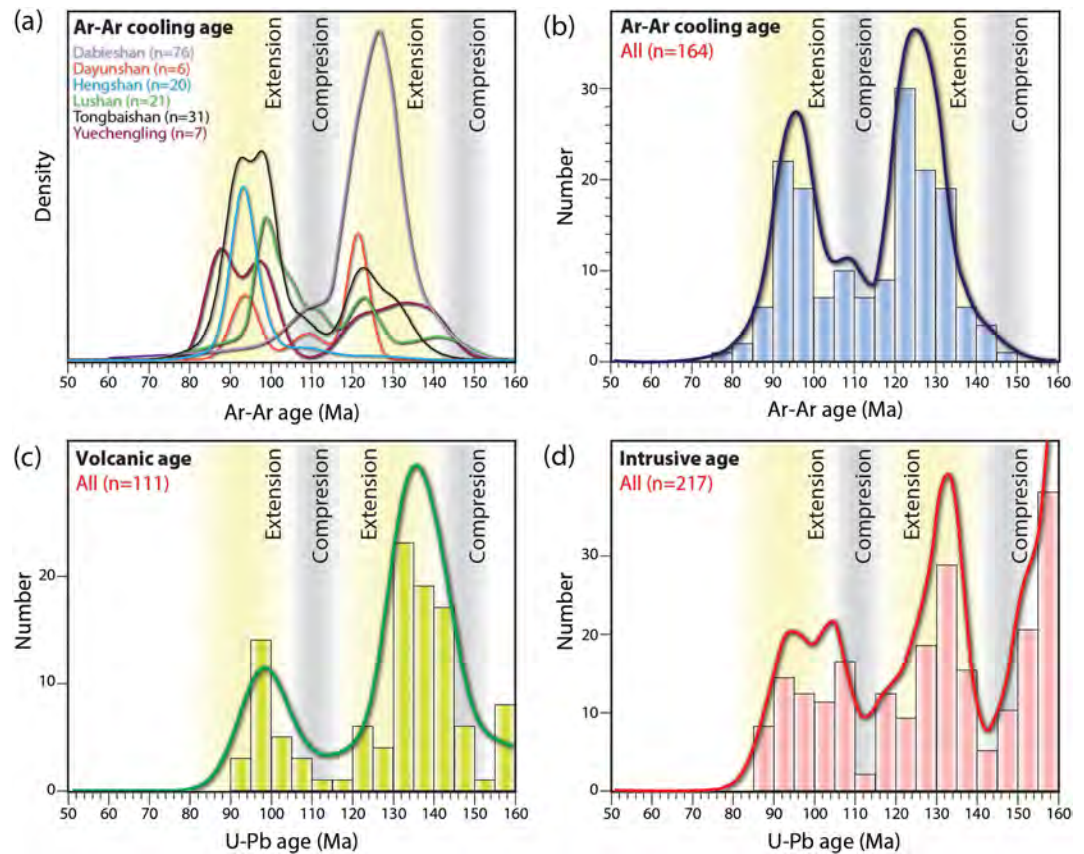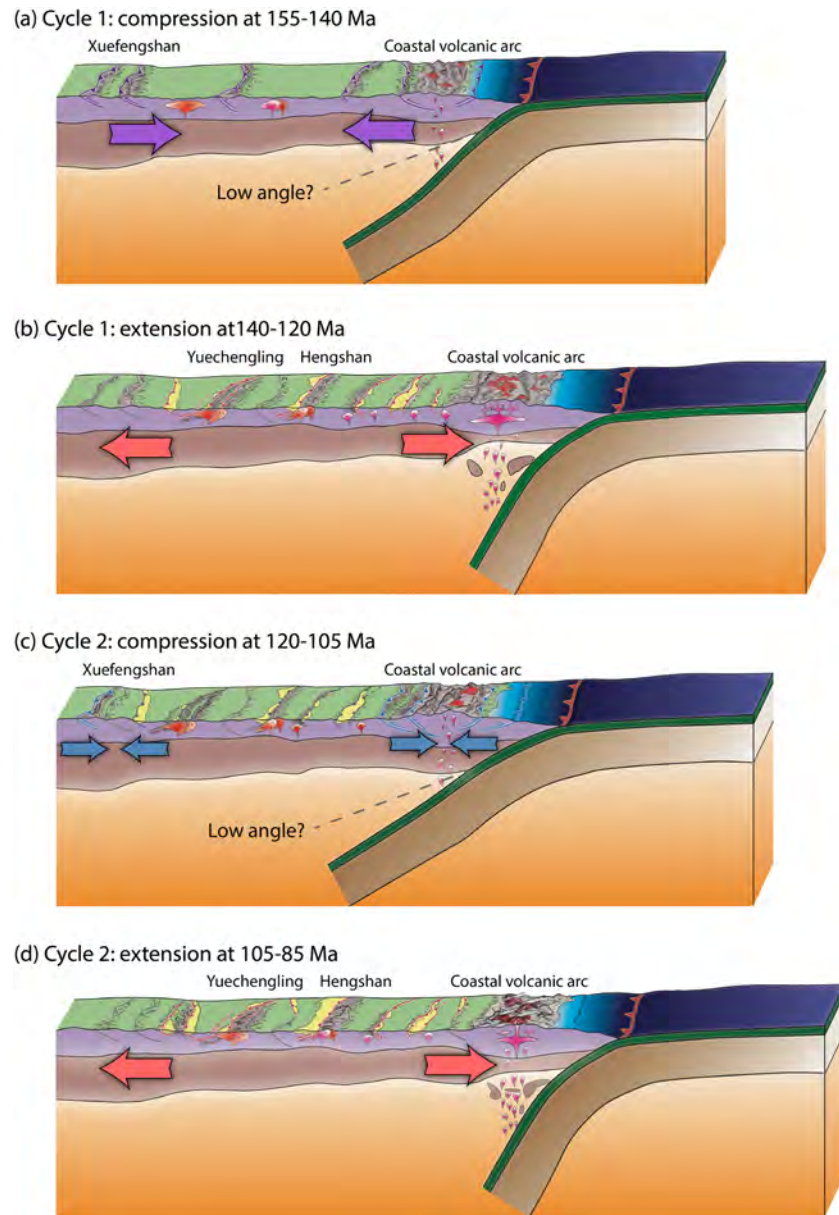
Figure 16. Age compilation of Cretaceous deformation, volcanism and plutonism. Note that a good correlation between peaks/trough (cooling ages, volcanic ages, and intrusive ages) and extensional/compressional events is well documented. (a) Density plot of ^{40}Ar-^{39}Ar cooling ages from extensional structures in the South China Block. (See references of each curve in the caption of Figure 15.) (b) Density plot of all ^{40}Ar-^{39}Ar cooling ages. (c and d) Density plot of volcanic and intrusive ages, respectively. Data are collected from synthesis of Li et al. (2014) and Jiang et al. (2015).

and 120–85 Ma, respectively. Each cycle is characterized by (i) compressional tectonics with magmatic quiescence and (ii) extensional tectonics with magmatic flare-up (Figure 16). The temporal-spatial relationship between magmatism and the subduction system has long been debated. Initially, the Cretaceous magmatism was considered as a continuous process with an eastward migration of intrusions correlated with the steepening of the subduction angle (Zhou & Li, 2000). Increasing geochronological and structural studies help better constrain the episodic magmatic events, including their precise temporal and spatial distributions. Accordingly, the geodynamics of the magmatic flare-ups and lulls were also discussed (Li et al., 2010; Li et al., 2014).

Based on these enlightening works, we can propose here a geodynamic scenario in attempt to discuss the tectonomagmatic cyclicity of the Paleo-Pacific subduction (Figure 17).

1. From 155 to 140 Ma, the SCB suffered intensive compression that produced intracontinental thrust belts from Xuefengshan to the eastern Sichuan Basin (Figures 15 and 17a). Those belts partly reactivated the faults formed during the Triassic orogeny and progressively migrated eastward (Chu et al., 2015; Chu, Faure, Lin, & Wang, 2012; Chu, Faure, Lin, Wang, & Ji, 2012; Li et al., 2012; Yan et al., 2003, 2009; Zhang et al., 2012). The contemporaneous magmatism was rare in the SCB. The first stage of extension (D₁) started at ~140 Ma that also coincided with the Early Cretaceous magmatic flare-up (Li et al., 2014; Zhou et al., 2006). The interaction between pluton emplacement and regional extension resulted in widespread domes (Figure 17b), exhuming middle crustal rocks, including high-temperature amphibolites and migmatites (Ji, Faure, et al., 2018; Li et al., 2012; Lin et al., 2000; Ratschbacher et al., 2000; Zhu, Xie, et al., 2010, and references therein). The extension terminated around 120 Ma that marks the end of the first compression-extension cycle.

(a) Cycle 1: compression at 155-140 Ma

(b) Cycle 1: extension at140-120 Ma

(c) Cycle 2: compression at 120-105 Ma

(d) Cycle 2: extension at 105-85 Ma

Figure 17. Three-dimensional views showing the tectonic evolution of the South China Block in the Izanagi/Paleo-Pacific subduction system. Two tectonomagmatic cycles with the succession of compression and extension regimes are also schematized. (a) Compressional stage of the first cycle that generated distributed thrust belts. (b) Extensional stage of the first cycle with a magmatic flare-up and extensional structures. (c) Compressional stage of the second cycle. Crustal shortening were localized in Xuefengshan and coastal regions. The West Philippine Block is not shown because it is out of the range of the section. (d) Extensional stage of the second cycle with reactivation of extensional structures of the first cycle and formation of new detachments. Note that the initiation of the second extension in the Yuechengling Massif is ~5 Myr later than the regional extension.

2. During the second cycle, a similar process from compression to extension is documented (Figures 17c and 17d). Localized ductile-brittle deformation at the eastern margin and center of the SCB induced thrusts and folds that involved the Early Cretaceous strata (Figure 17c), leading to tectonic inversion of Early Cretaceous basins (Chen, 2013; Li et al., 2012; Liang & Li, 2005; Wei et al., 2016). A Lower-Upper Cretaceous unconformity is also widespread in the SCB related to this compression (Li et al., 2014; Shu et al., 2009). The concurrent magmatism significantly decreased at 120–105 Ma, except in some parts of the arc volcanic belt (Li, 2000; Li et al., 2010). Subsequently, the entire subduction system reached an

extensional stage that gave rise to a 1,000-km-wide stretched region with widespread extension-related basins, domes/MCCs, and magmatism (Figure 17d). Such a tectonic scenario is similar to that described in the Cenozoic Basin and Range Province in the western United States (Davis & Lister, 1988; Dickinson, 2004; Sonder & Jones, 1999) or the Aegean Sea (Jolivet et al., 2013, 2018; Jolivet & Brun, 2010), where the lithosphere is highly extended to produce numerous MCCs and domes.

To interpret the tectonic switches in the Cretaceous, several models have been proposed, including changes of the subduction direction and the angle of the subducted slab (Ji, Chen, et al., 2018; Zhou et al., 2006; Zhou & Li, 2000). However, three switches of the subduction direction in such a short period (140–105 Ma) appear unlikely; and the mechanism for subduction angle is still disputed. A new model that requires the presence of exotic bodies on the subducting slab, such as a ridge, an oceanic plateau, or a continental slice, seems a plausible answer, because the positive topography and buoyancy can effectively shallow or deepen the subduction angle and thus produce compressional or extensional regimes in the overriding plate (Dickinson, 2004; Gutscher et al., 1999; Sun et al., 2007, 2010). As a matter of fact, such cyclical activity is a ubiquitous phenomenon in subduction zones (Dickinson, 2004; Jolivet & Brun, 2010; Kirsch et al., 2016), where intermittent compression and extension well illustrate the regional geological evolution. In the case of South China, a ridge on the Izanagi/Paleo-Pacific plate that entered into the Cretaceous subduction zone in East Asia led to a low angle or flat subduction that reduced the arc magmatism and caused crustal thickening (Li et al., 2014; Sun et al., 2007). After the consumption of this ridge, the subducting slab with normal buoyancy started to rollback, then the arc magmatism and a regional extensional stress field resumed. At ~120 Ma, the West Philippine Block entered into the subduction zone and collided with the SCB, generating compression at the SCB margin and transferred stress into the continental interior (Faure et al., 1989). Following the amalgamation of the two blocks, the restarted oceanic subduction generated the second phase of extension and arc magmatism.

There is an alternative way to trigger the episodic tectonic evolution of subduction zones, which does not necessitate flat subduction. Recent studies in the North American and South American Cordilleras shed new light on understanding the mechanism of repeated extension and magmatic flare-up (DeCelles et al., 2009, 2015). This model considers two major stages: (1) Retroarc underthrusting that leads to widespread intracontinental compression accommodates the convergence at the plate boundary and brings upper crustal, hydrous rocks into the region below the arc, thickening the crust and lithosphere. (2) Increased instability of the growing arc lithosphere gives rise to the foundering of the eclogitic root, which causes successive high-flux magmatism and isostatic rebound of the upper plate. This model can also better explain the tectonic evolution at the eastern margin of the SCB that includes episodic switches from compression to extension and from magmatic lulls to flare-ups. Furthermore, the correlation between convergence rates and stress regimes on the plate, in which high velocity corresponds to high-flux magmatism and regional extension (Engebretson et al., 1985), complies with the prediction of DeCelles et al. (2015). Despite the need for further investigation and tests, it is probable that the buoyant block and the retroarc underthrusting-arc root foundering may have both played crucial roles in the Cretaceous episodic evolution of the SCB.

8. Conclusions

Our multiscale structural analysis and geochronological data indicate that the YCL Massif experienced two stages of extension, both of which are characterized by intense ductile deformation with a top-to-the west shear sense. The first stage (~140–120 Ma) generates a narrow shear zone at the Tianhu Fault in the middle of the YCL pluton associated with low-temperature deformation microstructures and a limited activity of the Ziyuan Detachment at the western pluton margin. Along the Tianhu Fault, the Eastern YCL pluton was exhumed between 140 and 120 Ma. The second stage (100–85 Ma), which was also the main phase of extension, deformed the western part of the YCL pluton with penetrative low-angle foliation and lineation. The Tianhu Fault was reactivated at subsurface with brittle overprinting structures.

By integrating available structural data on the extensional structures in the SCB, the two-phase extension is explicitly recognized in two time spans, at 140–120 and 105–85 Ma. Both extensional events show a clear temporal relationship with volcanic and intrusive rocks of the arc magmatism, and follow the two compressional events at 155–140 and 120–105 Ma, constituting two compression-extension cycles. Our new data, together with published work, highlight a periodic change of stress regime that is intimately linked to the oceanic subduction. During the first cycle, the subduction of the Izanagi/Paleo-Pacific Plate ridge

decreased the subduction angle and triggered intracontinental contraction at 155–140 Ma. The subsequent slab rollback after the consumption of the ridge generated the Early Cretaceous extension and large magmatic activity at 140–120 Ma. The second cycle initiated the retroarc thrusting when the West Philippine Block collided with the SCB around 120–105 Ma. At 105–85 Ma, the extension resumed and controlled the stress field responsible for a climax of the dome/MCC formation and basin sedimentation in the SCB.

References

Augier, R., Jolivet, L., Gadenne, L., Lahfid, A., & Driussi, O. (2015). Exhumation kinematics of the Cycladic Blueschists unit and back-arc extension, insight from the Southern Cyclades (Sikinos and Folegandros Islands, Greece). *Tectonics*, *34*, 152–185. https://doi.org/10.1002/2014TC003664

Bureau of Geology and Mineral Resources of Guangxi Autonomous Region (BGMRGX) (1985). *Regional Geology of the Guangxi Autonomous region* (p. 851). Beijing: Geological Publishing House.

Bureau of Geology and Mineral Resources of Hunan Province (BGMRHN) (1988). *Regional Geology of the Hunan Province* (p. 507). Beijing: Geological Publishing House.

Bureau of Geology and Mineral Resources of Jiangxi Province (BGMRJX) (1984). *Regional Geology of the Jiangxi Province* (p. 921). Beijing: Geological Publishing House.

Bureau of Geology and Mineral Resources of Zhejiang Province (BGMRZJ) (1989). *Regional Geology of the Zhejiang Province* (p. 688). Beijing: Geological Publishing House.

Charvet, J., Lapierre, H., & Yu, Y. (1994). Geodynamic significance of the Mesozoic volcanism of southeastern China. *Journal of Southeast Asian Earth Sciences*, *9*(4), 387–396.

Charvet, J., Shu, L., Faure, M., Choulet, F., Wang, B., Lu, H., & Le Breton, N. (2010). Structural development of the Lower Paleozoic belt of South China: Genesis of an intracontinental orogen. *Journal of Asian Earth Sciences*, *39*(4), 309–330.

Chen, L., Cheng, C., & Wei, Z. G. (2009). Seismic evidence for significant lateral variations in lithospheric thickness beneath the central and western North China Craton. *Earth and Planetary Science Letters*, *286*, 171–183.

Chen, T., Niu, B., Liu, Z., Fu, Y., & Ren, J. (1992). Geochronology of Yanshanian magmatism and metamorphism in the Hinterland of the Dabie Mountains and their geologic implications. *Acta Geologica Sinica - English Edition*, *5*(2), 155–163.

Chen, Z. (2013). Early Mesozoic tectonic evolution in the south margin of South China block, Ph.D. thesis, Chinese Academy of Sciences, China, 192 pp.

Chu, Y., Faure, M., Lin, W., & Wang, Q. (2012). Early Mesozoic tectonics of the South China block: Insights from the Xuefengshan intracontinental orogen. *Journal of Asian Earth Sciences*, *61*, 199–220.

Chu, Y., Faure, M., Lin, W., Wang, Q., & Ji, W. (2012). Tectonics of the Middle Triassic intracontinental Xuefengshan Belt, South China: New insights from structural and chronological constraints on the basal décollement zone. *International Journal of Earth Sciences*, *101*(8), 2125–2150.

Chu, Y., & Lin, W. (2014). Phanerozoic polyorogenic deformation in southern Jiuling Massif, northern South China Block: Constraints from structural analysis and geochronology. *Journal of Asian Earth Sciences*, *86*, 117–130.

Chu, Y., & Lin, W. (2018). Strain analysis of the Xuefengshan Belt, South China: From internal strain variation to formation of the orogenic curvature. *Journal of Structural Geology*, *116*, 131–145.

Chu, Y., Lin, W., Faure, M., & Wang, Q. (2015). Early Mesozoic intracontinental orogeny: Example of the Xuefengshan-Jiuling Belt (in Chinese with English abstract). *Acta Petrologica Sinica*, *31*(8), 2145–2155.

Chu, Y., Lin, W., Faure, M., Wang, Q., & Ji, W. (2012). Phanerozoic tectonothermal events of the Xuefengshan Belt, central South China: Implications from U-Pb age and Lu-Hf determinations of granites. *Lithos*, *150*, 243–255.

Crittenden, M. D., Coney, P. J., & Davis, G. H. (Eds) (1980). Cordilleran metamorphic core complexes. *Geological Society of America Memoir*, *153*, 490.

Cui, J., Liu, X., Dong, S., & Hu, J. (2012). U–Pb and ^{40}Ar/^{39}Ar geochronology of the Tongbai complex, central China: Implications for Cretaceous exhumation and lateral extrusion of the Tongbai–Dabie HP/UHP terrane. *Journal of Asian Earth Sciences*, *47*, 155–170.

Davis, G. A., & Lister, G. S. (1988). Detachment faulting in continental extension: Perspectives from the Southwestern U.S. Cordillera. In S. P. Clark, Jr., et al. (Eds.), *Processes in continental lithospheric deformation*, *Geological Society of America Special Paper* (Vol. 218, pp. 133–159).

Davis, G. H., & Coney, P. J. (1979). Geologic development of the Cordilleran metamorphic core complexes. *Geology*, *7*(3), 120–124.

DeCelles, P. G., Ducea, M. N., Kapp, P., & Zandt, G. (2009). Cyclicity in Cordilleran orogenic systems. *Nature Geosciences*, *2*(4), 251–257.

DeCelles, P. G., Zandt, G., Beck, S. L., Currie, C. A., Ducea, M. N., Kapp, P., et al. (2015). Cyclical orogenic processes in the Cenozoic central Andes. In P. G. DeCelles, M. N. Ducea, B. Carrapa, & P. A. Kapp (Eds.), *Geodynamics of a Cordilleran orogenic system: The Central Andes of Argentina and Northern Chile*, *Geological Society of America Memoir* (Vol. 212, pp. 459–490). https://doi.org/10.1130/2015.1212(22)

Dickinson, W. R. (2004). Evolution of the North American Cordillera. *Annual Review of Earth and Planetary Sciences*, *32*(1), 13–45.

Dodson, M. H. (1973). Closure temperature in cooling geochronological and petrological systems. *Contributions to Mineralogy and Petrology*, *40*(3), 259–274.

Dong, S., Gao, R., Yin, A., Guo, T., Zhang, Y., Hu, J., et al. (2013). What drove continued continent-continent convergence after ocean closure? Insights from high-resolution seismic-reflection profiling across the Daba Shan in central China. *Geology*, *41*(6), 671–674.

Eide, E. A., McWilliams, M. O., & Liou, J. G. (1994). ^{40}Ar/^{39}Ar geochronology and exhumation of high-pressure to ultrahigh-pressure metamorphic rocks in east-central China. *Geology*, *22*, 601–604.

Engebretson, D. C., Cox, A., & Gordon, R. G. (Eds.). (1985). *Relative Motions Between Oceanic and Continental Plates in the Pacific Basin*. Boulder, CO: Geological Society of America.

Faure, M., Lin, W., Chu, Y., & Lepvrier, C. (2016). Triassic tectonics of the southern margin of the South China Block. *Comptes Rendus Geoscience*, *348*(1), 5–14.

Faure, M., Marchadier, Y., & Rangin, C. (1989). Pre-Eocene synmetamorphic structure in the Mindoro-Romblon-Palawan Area, West Philippines, and implications for the history of Southeast-Asia. *Tectonics*, *8*(5), 963–979.

Faure, M., Shu, L., Wang, B., Charvet, J., Choulet, F., & Monié, P. (2009). Intracontinental subduction: A possible mechanism for the Early Palaeozoic Orogen of SE China. *Terra Nova*, *21*(5), 360–368.

Faure, M., Sun, Y., Shu, L., Monié, P., & Charvet, J. (1996). Extensional tectonics within a subduction-type orogen. The case study of the Wugongshan dome (Jiangxi Province, southeastern China). *Tectonophysics*, *263*(1-4), 77–106.

Gutscher, M. A., Olivet, J. L., Aslanian, D., Eissen, J. P., & Maury, R. (1999). The "lost inca plateau": cause of flat subduction beneath Peru? *Earth and Planetary Science Letters*, *171*(3), 335–341.

Hacker, B. R., Ratschbacher, L., Webb, L., McWilliams, M. O., Ireland, T., Calvert, A., et al. (2000). Exhumation of ultrahigh-pressure continental crust in east central China: Late Triassic-Early Jurassic tectonic unroofing. *Journal of Geophysical Research*, *105*(B6), 13,339–13,364.

Hacker, B. R., & Wang, Q. C. (1995). Ar/Ar geochronology of ultrahigh-pressure metamorphism in central China. *Tectonics*, *14*(4), 994–1006.

Hou, Q. L., Liu, Q., Li, J., & Zhang, H. Y. (2007). Late Mesozoic shear zones and its chronology in the Dabie Mountains, central China (in Chinese with English abstract). *Chinese Journal of Geology*, *42*, 114–123.

Ji, W., Chen, Y., Chen, K., Wei, W., Faure, M., & Lin, W. (2018). Multiple emplacement and exhumation history of the Late Mesozoic Dayunshan-Mufushan Batholith in Southeast China and its tectonic significance: 2. Magnetic fabrics and gravity survey. *Journal of Geophysical Research: Solid Earth*, *123*, 711–731. https://doi.org/10.1002/2017JB014598

Ji, W., Faure, M., Lin, W., Chen, Y., Chu, Y., & Xue, Z. (2018). Multiple emplacement and exhumation history of the Late Mesozoic Dayunshan-Mufushan Batholith in Southeast China and its tectonic significance: 1. Structural analysis and geochronological constraints. *Journal of Geophysical Research: Solid Earth*, *113*, 689–710. https://doi.org/10.1002/2017JB014597

Ji, W., Lin, W., Faure, M., Chen, Y., Chu, Y., & Xue, Z. (2017). Origin of the Late Jurassic to Early Cretaceous peraluminous granitoids in the northeastern Hunan province (middle Yangtze region), South China: Geodynamic implications for the Paleo-Pacific subduction. *Journal of Asian Earth Sciences*, *141*, 174–193.

Ji, W., Lin, W., Faure, M., Chu, Y., Wu, L., Wang, F., et al. (2014). Origin and tectonic significance of the Huangling massif within the Yangtze craton, South China. *Journal of Asian Earth Sciences*, *86*, 59–75.

Ji, W., Lin, W., Faure, M., Shi, Y., & Wang, Q. (2017). The early Cretaceous orogen-scale Dabieshan metamorphic core complex: Implications for extensional collapse of the Triassic HP–UHP orogenic belt in east-central China. *International Journal of Earth Sciences*, *106*(4), 1311–1340.

Jiang, X. Y., Li, X. H., Collins, W. J., & Huang, H. Q. (2015). U-Pb age and Hf-O isotopes of detrital zircons from Hainan Island: Implications for Mesozoic subduction models. *Lithos*, *239*, 60–70.

Jolivet, L., & Brun, J. P. (2010). Cenozoic geodynamic evolution of the Aegean. *International Journal of Earth Sciences*, *99*(1), 109–138.

Jolivet, L., Faccenna, C., Huet, B., Labrousse, L., Le Pourhiet, L., Lacombe, O., et al. (2013). Aegean tectonics: Strain localisation, slab tearing and trench retreat. *Tectonophysics*, *597-598*, 1–33.

Jolivet, L., Menant, A., Clerc, C., Sternai, P., Bellahsen, N., Leroy, S., et al. (2018). Extensional crustal tectonics and crust-mantle coupling, a view from the geological record. *Earth-Science Reviews*, *185*, 1187–1209.

Kirsch, M., Paterson, S. R., Wobbe, F., Martinez Ardila, A. M., Clausen, B. L., & Alasion, P. H. (2016). Temporal histories of Cordilleran continental arcs: Testing models for magmatic episodicity. *American Mineralogist*, *101*, 2133–2154.

Koppers, A. A. P. (2002). ArArCALC—Software for ^{40}Ar/^{39}Ar age calculations. *Computer & Geosciences*, *28*, 605–619. https://doi.org/10.1016/S0098-3004(01)00095-4

Law, R. D. (2014). Deformation thermometry based on quartz c-axis fabrics and recrystallization microstructures: A review. *Journal of Structural Geology*, *66*, 129–161.

Li, J., Zhang, Y., Dong, S., & Johnston, S. T. (2014). Cretaceous tectonic evolution of South China: A preliminary synthesis. *Earth-Science Reviews*, *134*, 98–136.

Li, J., Zhang, Y., Dong, S., Su, J., Li, Y., Cui, J., & Shi, W. (2013). The Hengshan low-angle normal fault zone: Structural and geochronological constraints on the Late Mesozoic crustal extension in South China. *Tectonophysics*, *606*, 97–115.

Li, J. H., Dong, S. W., Yin, A., Zhang, Y. Q., & Shi, W. (2015). Mesozoic tectonic evolution of the Daba Shan Thrust Belt in the southern Qinling orogen, central China: Constraints from surface geology and reflection seismology. *Tectonics*, *34*, 1545–1575. https://doi.org/10.1002/2014TC003813

Li, J. H., Shi, W., Zhang, Y., Dong, S., & Ma, Z. (2016). Thermal evolution of the Hengshan extensional dome in central South China and its tectonic implications: New insights into low-angle detachment formation. *Gondwana Research*, *35*, 425–441.

Li, J. H., Zhang, Y. Q., Dong, S. W., & Li, H. L. (2012). Late Mesozoic–Early Cenozoic deformation history of the Yuanma Basin, central South China. *Tectonophysics*, *570–571*, 163–183.

Li, X. H. (2000). Cretaceous magmatism and lithospheric extension in Southeast China. *Journal of Asian Earth Sciences*, *18*(3), 293–305.

Li, Z. X., & Li, X. H. (2007). Formation of the 1300-km-wide intracontinental orogen and postorogenic magmatic province in Mesozoic South China: A flat-slab subduction model. *Geology*, *35*(2), 179–182.

Li, Z. X., Li, X. H., Wartho, J. A., Clark, C., Li, W. X., Zhang, C. L., & Bao, C. (2010). Magmatic and metamorphic events during the early Paleozoic Wuyi-Yunkai orogeny, southeastern South China: New age constraints and pressure-temperature conditions. *Geological Society of America Bulletin*, *122*(5-6), 772–793.

Liang, X. Q., & Li, X. H. (2005). Late Permian to Middle Triassic sedimentary records in Shiwandashan Basin: Implication for the Indosinian Yunkai Orogenic Belt, South China. *Sedimentary Geology*, *177*(3-4), 297–320.

Lin, W., Charles, N., Chen, Y., Chen, K., Faure, M., Wu, L., et al. (2013). Late Mesozoic compressional to extensional tectonics in the Yiwulüshan massif, NE China and their bearing on the Yinshan–Yanshan orogenic belt: Part II: Anisotropy of magnetic susceptibility and gravity modeling. *Gondwana Research*, *23*(1), 78–94.

Lin, W., Enami, M., Faure, M., Scharer, U., & Arnaud, N. (2007). Survival of eclogite xenolith in a Cretaceous granite intruding the Central Dabieshan migmatite gneiss dome (Eastern China) and its tectonic implications. *International Journal of Earth Sciences*, *96*(4), 707–724.

Lin, W., Faure, M., Chen, Y., Ji, W., Wang, F., Wu, L., et al. (2013). Late Mesozoic compressional to extensional tectonics in the Yiwulüshan massif, NE China and its bearing on the evolution of the Yinshan–Yanshan orogenic belt: Part I: Structural analyses and geochronological constraints. *Gondwana Research*, *23*(1), 54–77.

Lin, W., Faure, M., Monié, P., Scharer, U., & Panis, D. (2008). Mesozoic extensional tectonics in eastern Asia: The South Liaodong Peninsula metamorphic core complex (NE China). *The Journal of Geology*, *116*(2), 134–154.

Lin, W., Faure, M., Monié, P., Scharer, U., Zhang, L. S., & Sun, Y. (2000). Tectonics of SE China: New insights from the Lushan massif (Jiangxi Province). *Tectonics*, *19*(5), 852–871.

Lin, W., & Wang, Q. C. (2006). Late Mesozoic extensional tectonics in the North China Block: A crustal response to subcontinental mantle removal? *Bulletin de la Société Géologique de France*, *177*(6), 287–297.

Lin, W., & Wei, W. (2019). Late Mesozoic extensional tectonics in the North China Craton and its adjacent regions: A review and synthesis. *International Geology Review*. https://doi.org/10.1080/00206814.2018.1477073

Lister, G. S., Banga, G., & Feenstra, A. (1984). Metamorphic core complexes of Cordilleran type in the Cyclades, Aegean Sea, Greece. *Geology*, *12*(4), 221–225.

Lister, G. S., & Davis, G. A. (1989). The origin of metamorphic core complexes and detachment faults formed during Tertiary continental extension in the northern Colorado River region, U.S.A. *Journal of Structural Geology*, *11*(1), 65–94.

Liu, J., Davis, G. A., Lin, Z., & Wu, F. (2005). The Liaonan metamorphic core complex, Southeastern Liaoning Province, North China: A likely contributor to Cretaceous rotation of Eastern Liaoning, Korea and contiguous areas. *Tectonophysics*, *407*(1–2), 65–80.

Liu, J., Mao, J. W., Ye, H. S., Xie, G. Q., Yang, G. Q., & Zhang, W. (2008). Zircon LA-ICPMS U-Pb dating of Hukeng granite in Wugongshan area, Jiangxi Province and its geochemical characteristics. *Acta Petrologica Sinica*, *24*(8), 1813–1822.

Lou, F., Shen, W., Wang, D., Shu, L., Wu, F., Zhang, F., & Yu, J. (2005). Zircon U-Pb isotopic chronology of the Wugongshan Dome compound granite in Jiangxi Province. *Acta Geological Sinica*, *79*(5), 636–644.

Passchier, C. W., & Trouw, R. A. J. (2005). *Microtectonics* (2nd ed., pp. 27–66). Berlin: Springer.

Ratschbacher, L., Hacker, B. R., Webb, L. E., McWilliams, M., Ireland, T., Dong, S., et al. (2000). Exhumation of the ultrahigh-pressure continental crust in east central China: Cretaceous and Cenozoic unroofing and the Tan-Lu fault. *Journal of Geophysical Research*, *105*(B6), 13,303–13,338.

Ren, J. S., Chen, T. Y., Niu, B. G., Liu, Z. G., & Liu, F. R. (1990). *Tectonic evolution of the continental lithosphere and metallogeny in eastern China and adjacent areas* (p. 205). Beijing: Science Press.

Ring, U., Glodny, J., Will, T., & Thomson, S. (2010). The Hellenic subduction system: High-pressure metamorphism, exhumation, normal faulting, and large-scale extension. *Annual Review of Earth and Planetary Sciences*, *38*(1), 45–76.

Shu, L., & Charvet, J. (1996). Kinematics and geochronology of the Proterozoic Dongxiang-Shexian ductile shear zone: With HP metamorphism and ophiolitic melange (Jiangnan Region, South China). *Tectonophysics*, *267*(1-4), 291–302.

Shu, L. S., Zhou, X. M., Deng, P., Wang, B., Jiang, S. Y., Yu, J. H., & Zhao, X. X. (2009). Mesozoic tectonic evolution of the Southeast China Block: New insights from basin analysis. *Journal of Asian Earth Sciences*, *34*(3), 376–391.

Sonder, L. J., & Jones, C. H. (1999). Western United States extension: How the West was widened. *Annual Review of Earth and Planetary Sciences*, *27*, 417–462.

Stipp, M., Stuitz, H., Heilbronner, R., & Schmid, S. M. (2002). The eastern Tonale fault zone: A natural laboratory' for crystal plastic deformation of quartz over a temperature range from 250 to 700 °C. *Journal of Structural Geology*, *24*(12), 1861–1884.

Sun, W. D., Ding, X., Hu, Y. H., & Li, X. H. (2007). The golden transformation of the Cretaceous plate subduction in the west Pacific. *Earth and Planetary Science Letters*, *262*(3–4), 533–542.

Sun, W. D., Ling, M. X., Yang, X. Y., Fan, W. M., Ding, X., & Liang, H. Y. (2010). Ridge subduction and porphyry copper–gold mineralization: An overview. *Science China-Earth Science*, *53*(4), 475–484.

Tian, Y., Kohn, B. P., Phillips, D., Hu, S., Gleadow, A. J. W., & Carter, A. (2016). Late Cretaceous–earliest Paleogene deformation in the Longmen Shan fold-and-thrust belt, eastern Tibetan Plateau margin: Pre-Cenozoic thickened crust? *Tectonics*, *35*, 2293–2312. https://doi.org/10.1002/2016TC004182

Wang, F., Wang, Q., Lin, W., Wu, L., Shi, W., Feng, H., & Zhu, R. (2014). 40Ar/39Ar geochronology of the North China and Yangtze Cratons: New constraints on Mesozoic cooling and cratonic destruction under East Asia. *Journal of Geophysical Research: Solid Earth*, *119*, 3700–3721. https://doi.org/10.1002/2013JB010708

Wang, F., Zheng, X. S., Lee, J. I. K., Choe, W. H., Evans, N., & Zhu, R. X. (2009). An 40Ar/39Ar geochronology on a mid-Eocene igneous event on the Barton and Weaver peninsulas: Implications for the dynamic setting of the Antarctic Peninsula. *Geochemistry, Geophysics, Geosystems*, *10*, Q12006. https://doi.org/10.1029/2009GC002874

Wang, J. L., He, B., & Guan, J. P. (2013). Study on age and mechanism of the metamorphism of the Xingzi Group in the Lushan Area, Jiangxi Province (in Chinese with English abstract). *Geotectonica et Metallogenia*, *138*(8), 489–498.

Wang, T., Zheng, Y., Zhang, J., Zeng, L., Donskaya, T., Guo, L., & Li, J. (2011). Pattern and kinematic polarity of late Mesozoic extension in continental NE Asia: Perspectives from metamorphic core complexes. *Tectonics*, *30*, TC6007. https://doi.org/10.1029/2011TC002896

Wang, W., Zhou, M. F., Yan, D. P., Li, L., & Malpas, J. (2013). Detrital zircon record of Neoproterozoic active-margin sedimentation in the eastern Jiangnan Orogen, South China. *Precambrian Research*, *235*, 1–19.

Wang, Y., Cui, J., Zhang, Y., Dong, S., Qi, W., Su, J., et al. (2015). Two-stage Cretaceous exhumation of Hengshan Complex in Hunan Province, SE China: Constraints arising from ^{40}Ar–^{39}Ar geochronology and Cretaceous tectonic implications. *Acta Geologica Sinica-English Edition*, *89*(6), 1869–1881.

Wang, Y., Wu, C., Zhang, A., Fan, W., Zhang, Y., Zhang, Y., et al. (2012). Kwangsian and Indosinian reworking of the eastern South China Block: Constraints on zircon U–Pb geochronology and metamorphism of amphibolites and granulites. *Lithos*, *150*, 227–242.

Wang, Y., Xiang, B., Zhu, G., & Jiang, D. (2011). Structural and geochronological evidence for Early Cretaceous orogen-parallel extension of the ductile lithosphere in the northern Dabie orogenic belt, East China. *Journal of Structural Geology*, *33*(3), 362–380.

Webb, L. E., Hacker, B. R., Ratschbacher, L., McWilliams, M. O., & Dong, S. (1999). Thermochronologic constraints on deformation and cooling history of high- and ultrahigh-pressure rocks in the Qinling-Dabie orogen, eastern China. *Tectonics*, *18*(4), 621–638.

Wei, W., Chen, Y., Faure, M., Martelet, G., Lin, W., Wang, Q., et al. (2016). An early extensional event of the South China Block during the Late Mesozoic recorded by the emplacement of the Late Jurassic syntectonic Hengshan Composite Granitic Massif (Hunan, SE China). *Tectonophysics*, *672–673*, 50–67.

Wei, W., Chen, Y., Faure, M., Shi, Y. H., Martelet, G., Hou, Q. L., et al. (2014). A multidisciplinary study on the emplacement mechanism of the Qingyang–Jiuhua Massif in Southeast China and its tectonic bearings. Part I: Structural geology, AMS and paleomagnetism. *Journal of Asian Earth Sciences*, *86*, 76–93.

Wei, W., Faure, M., Chen, Y., Ji, W., Lin, W., Wang, Q., et al. (2015). Back-thrusting response of continental collision: Early Cretaceous NW-directed thrusting in the Changle-Nan'ao belt (Southeast China). *Journal of Asian Earth Sciences*, *100*, 98–114.

Wei, W., Martelet, G., Le Breton, N., Shi, Y., Faure, M., Chen, Y., et al. (2014). A multidisciplinary study of the emplacement mechanism of the Qingyang–Jiuhua massif in Southeast China and its tectonic bearings. Part II: Amphibole geobarometry and gravity modeling. *Journal of Asian Earth Sciences*, *86*, 94–105.

Wernicke, B. (1981). Low-angle normal faults in the Basin and Range Province: Nappe tectonics in an extending orogen. *Nature*, *291*(5817), 645–648.

Wu, F.-Y., Yang, J.-H., Xu, Y.-g., Wilde, S. A., & Walker, R. J. (2019). Destruction of the North China Craton in the Mesozoic. *Annual Review of Earth and Planetary Sciences*, *47*, 173–195.

Wu, J., Liang, H., Huang, W., Wang, C., Sun, W., Sun, Y., et al. (2012). Indosinian isotope ages of plutons and deposits in southwestern Miaoershan-Yuechengling, northeastern Guangxi and implications on Indosinian mineralization in South China. *Chinese Science Bulletin*, *57*(9), 1024–1035.

Xu, G., & Wang, E. (2010). The uplift mechanism of Tongbai complex in Mesozoic and its coupling relationship with Nanyang Basin (in Chinese with English abstract). *Chinese Journal of Geology*, *45*(3), 626–652.

Xue, Z., Martelet, G., Lin, W., Faure, M., Chen, Y., Wei, W., et al. (2017). Mesozoic crustal thickening of the Longmenshan Belt (NE Tibet, China) by imbrication of basement slices: Insights from structural analysis, petrofabric and magnetic fabric studies and gravity modeling. *Tectonics*, *36*, 3110–3134. https://doi.org/10.1002/2017TC004754

Yan, D. P., Zhang, B., Zhou, M. F., Wei, G., Song, H. L., & Liu, S. F. (2009). Constraints on the depth, geometry and kinematics of blind detachment faults provided by fault-propagation folds: An example from the Mesozoic fold belt of South China. *Journal of Structural Geology*, *31*(2), 150–162.

Yan, D. P., Zhou, M. F., Li, S. B., & Wei, G. Q. (2011). Structural and geochronological constraints on the Mesozoic-Cenozoic tectonic evolution of the Longmen Shan thrust belt, eastern Tibetan Plateau. *Tectonics*, *30*, TC6005. https://doi.org/10.1029/2011tc002867

Yan, D. P., Zhou, M. F., Song, H., & Fu, Z. (2003). Structural style and tectonic significance of the Jianglang dome in the eastern margin of the Tibetan Plateau, China. *Journal of Structural Geology*, *25*(5), 765–779.

Yang, F., Song, C. Z., Ren, S. L., Li, J. H., Li, H. L., & Wang, W. (2017). Transition of Yanshanian Two-period tectonic property in the eastern detachment belt of Lushan metamorphic core complex: Evidence from Zircon U-Pb dating (in Chinese with English abstract). *Geological Review*, *63*(3), 581–596.

Zhang, Y. Q., Dong, S. W., Li, J. H., Cui, J. J., Su, J. B., & Li, Y. (2012). The new progress in the study of Mesozoic tectonics of South China (in Chinese with English abstract). *Acta Geoscientica Sinica*, *33*(3), 257–279.

Zhao, K. D., Jiang, S. Y., Sun, T., Chen, W. F., Ling, H. F., & Chen, P. R. (2013). Zircon U–Pb dating, trace element and Sr–Nd–Hf isotope geochemistry of Paleozoic granites in the Miao'ershan–Yuechengling batholith, South China: Implication for petrogenesis and tectonic–magmatic evolution. *Journal of Asian Earth Sciences*, *74*, 244–264.

Zhou, X. M., & Li, W. X. (2000). Origin of Late Mesozoic igneous rocks in Southeastern China: Implications for lithosphere subduction and underplating of mafic magmas. *Tectonophysics*, *326*(3-4), 269–287.

Zhou, X. M., Sun, T., Shen, W. Z., Shu, L. S., & Niu, Y. L. (2006). Petrogenesis of Mesozoic granitoids and volcanic rocks in South China: A response to tectonic evolution. *Episodes*, *29*(1), 26–33.

Zhu, G., Chen, Y., Jiang, D., & Lin, S. (2015). Rapid change from compression to extension in the North China Craton during the Early Cretaceous: Evidence from the Yunmengshan metamorphic core complex. *Tectonophysics*, *656*, 91–110.

Zhu, G., Wang, Y., Liu, G., Niu, M., Xie, C., & Li, C. (2005). $^{40}Ar/^{39}Ar$ dating of strike-slip motion on the Tan-Lu fault zone, East China. *Journal of Structural Geology*, *27*(8), 1379–1398.

Zhu, G., Xie, C. L., Chen, W., Xiang, B. W., & Hu, Z. Q. (2010). Evolution of the Hongzhen metamorphic core complex: Evidence for Early Cretaceous extension in the eastern Yangtze craton, eastern China. *Geological Society of America Bulletin*, *122*(3-4), 506–516.

Zhu, Q. B., Yang, K. G., & Wang, Y. (2010). Extensional detachment and magmatism of the Lushan metamorphic core complex: Constraints from $^{40}Ar/^{39}Ar$ and U–Pb geochronology (in Chinese with English abstract). *Geotectonica et Metallogenia*, *34*, 391–401.

Zhu, R., Chen, L., Wu, F., & Liu, J. (2011). Timing, scale and mechanism of the destruction of the North China Craton. *Science China-Earth Science*, *54*(6), 789–797.